Princeton Plasma Physics Laboratory

PPPL-4265
PPPL-4265

Physics Design for ARIES-CS

L.P. Ku, P.R. Garabedian, J. Lyon, A. Turnbull,
A. Grossman, T.K. Mau, M. Zarnstorff,
and the ARIES Team

October 2007

Prepared for the U.S. Department of Energy under Contract DE-AC02-76CH03073.

Princeton Plasma Physics Laboratory
Report Disclaimers

Full Legal Disclaimer

Trademark Disclaimer

PPPL Report Availability

Princeton Plasma Physics Laboratory:

http://www.pppl.gov/techreports.cfm

Office of Scientific and Technical Information (OSTI):

http://www.osti.gov/bridge

Related Links:

U.S. Department of Energy

Office of Scientific and Technical Information

Fusion Links

PHYSICS DESIGN FOR ARIES-CS

L. P. Ku[a], P. R. Garabedian[b], J. Lyon[c], A. Turnbull[d], A. Grossman[e], T. K. Mau[e],

M. Zarnstorff[a] and the ARIES Team

[a]*Princeton Plasma Physics Laboratory, Princeton University, Princeton, NJ 08543*

[b]*Courant Institute of Mathematical Sciences, New York University, NY, NY 10012*

[c]*Oak Ridge National Laboratory, Oak Ridge, TN 37831*

[d]*General Atomics, San Diego, CA 92186*

[e]*University of California, San Diego, San Diego, CA 92093*

Abstract

Novel stellarator configurations have been developed for ARIES-CS. These configurations are optimized to provide good plasma confinement and flux surface integrity at high beta. Modular coils have been designed for them in which the space needed for the breeding blanket and radiation shielding was specifically targeted such that reactors generating GW electrical powers would require only moderate major radii (<10 m). These configurations are quasi-axially symmetric in the magnetic field topology and have small number of field periods (≤3) and low aspect ratios (≤6). The baseline design chosen for detailed systems and power plant studies has 3 field periods, aspect ratio 4.5 and major radius 7.5 m operating at β~6.5% to yield 1 GW electric power. The shaping of the plasma accounts for ≥75% of the rotational transform. The effective

helical ripples are very small (< 0.6% everywhere) and the energy loss of alpha particles is calculated to be ≤5% when operating in high density regimes. An interesting feature in this configuration is that instead of minimizing all residues in the magnetic spectrum, we preferentially retained a small amount of the non-axisymmetric mirror field. The presence of this mirror and its associated helical field alters the ripple distribution, resulting in the reduced ripple-trapped loss of alpha particles despite the long connection length in a tokamak-like field structure. Additionally, we discuss two other potentially attractive classes of configurations, both quasi-axisymmetric: one with only two field periods, very low aspect ratios (~2.5), and less complex coils, and the other with the plasma shaping designed to produce low shear rotational transform so as to assure the robustness and integrity of flux surfaces when operating at high β.

I. INTRODUCTION

ARIES-CS is aimed at investigating the feasibility, cost competitiveness and physics and engineering issues of using compact stellarators as the core for power producing fusion reactors.

Stellarators are inherently steady-state devices known to be resilient to MHD perturbations. Data from LHD and W7AS experiments have provided ample support for this proposition [1, 2]. Predictions of beta limit based on the linear, ideal MHD stability analysis have been exceeded frequently in experiments, although nonlinear analysis has performed better. The poloidal flux provided by external coils supports the rotational transform, making stellarators virtually free of plasma disruptions. In recent years the technique of drift orbit optimization in which the collisionless particle trajectories may be made well confined has been widely explored. The concept was introduced by Boozer [3] who showed that expressed in "Boozer" coordinates drift trajectories depended only on the local magnetic field strength, $1/|B|^2$, not the vector components of the field. The freedom of being able to use the three-dimensional geometry to shape plasmas in stellarators can be exploited to achieve certain topological symmetry of the magnetic field strength in the plasma. Nuehrenberg et al. were the first to demonstrate that plasmas with quasi-helical symmetry could be constructed in this way [4]. A quasi-helically symmetric stellarator, HSX, has been built and is operational at the University of Wisconsin, Madison [5]. Nuehrenberg, Lotz and Gori have further shown that non-axisymmetric fields can be constructed in which |B| is independent of toroidal angles in Boozer coordinates [6], demonstrating the feasibility of constructing quasi-axially symmetric (QAS) configurations. A quasi-axially symmetric experiment along these lines

has been proposed [7] and the modular Helias-like Heliac (MHH) configurations were developed for the Stellarator Power Plant Studies (SPPS) [8, 9]. The NCSX stellarator [10] is under construction at the Princeton Plasma Physics Laboratory and experiments are expected to commence in 2009. Another optimized stellarator, QPS, which was proposed on the basis of quasi-poloidal symmetry, is being considered at Oak Ridge National Laboratory [11]. W7X, which is under construction in Greifswald, Germany, is also an optimized stellarator but it uses the concept of quasi-isodynamicity and linked mirrors [12]. These optimized stellarators are expected to have stable plasmas with good confinement, raising the prospect that fusion reactors may be designed with good particle orbit confinement typically found in tokamaks and MHD stable plasmas typically found in stellarators but without the need to have elaborate feedback controls and large amount of re-circulating power.

Stellarator fusion reactors have been studied in the past, but all of them are large in comparison to the plants based on toroidally symmetric power cores. For example, FFHR [13], a reactor based on the concept of LHD, has major radius ~14 m; HSR [14], a reactor based on W7X, ~18 m; and SPPS [9], a four field period, quasi-axially symmetric concept, 14 m. Our challenge is to make stellarator power plants competitive in size and cost to tokamak based power plants without compromising the desirable physics properties and engineering requirements. To achieve this objective we have concentrated on QAS configurations with small aspect ratios. If the magnetic field strength can be made truly axially symmetric in magnetic coordinates, then the particle drift orbits will look exactly the same as a tokamak and particles will be well confined, as in a tokamak. On the other hand, as aspect ratio becomes smaller the toroidal mode coupling has less

effect on the symmetry properties of the axially symmetric configurations. These QAS configurations can be designed with aspect ratios, average ellipticity and triangularity similar to the advanced tokamaks. The plasma is expected to be able to rotate freely in the direction of quasi-axisymmetry, allowing one to apply the same technique for transport barrier formation as in tokamaks. Due to the quasi-axisymmetry, the neoclassical bootstrap current is similar to tokamaks, but the magnitude is reduced by the higher rotational transform. The low aspect ratio QAS configurations therefore tend to be like hybrids between tokamaks and conventional stellarators.

These positive traits of stellarator power plants have to be balanced by the complexities they introduce by virtue of lacking the geometric symmetry. The feasibility of remotely maintaining the machine in a reactor environment must be ascertained and the cost associated with the increased complexity must be controlled. A machine of smaller size may be realized if we can find a configuration of small aspect ratio that is stable at high beta. However, in deuterium-tritium (DT) reactors, because tritium breeding is required to maintain the fuel self-sufficiency and shielding is required to protect the coils from radiation damage and nuclear heating, consideration given solely on the basis of plasma properties is not adequate. One has to be able to find coils that are not only capable of producing plasmas with the desirable properties but also are sufficiently away from the plasma to provide enough room for the blanket and shielding. Because the high order harmonics of magnetic fields decay rapidly, it may not always be feasible to place coils at an arbitrary distance from the plasma. Coil design in stellarators is an integral part of the configuration development. The singly most important figure of merit for a power plant is the cost of electricity (COE), and to reduce COE the plant size

is one of the most important parameters in the design optimization. The plant size is directly related to the separation between the last closed magnetic surface and the coils. It is our goal to construct a compact reactor system consisting of an optimized compact stellarator core and a compact set of coils in a coherent and consistent manner.

The development of the ARIES-CS configurations naturally evolved from the design of NCSX. We have identified two most critical issues we need to address when extending NCSX to a reactor—the separation distance between coils and plasma and the energy loss of alpha particles. The efforts to improve designs in these two areas led to the plasma configuration, N3ARE, and coil configuration, KZD, that were chosen as the baseline for systems and detailed engineering studies. In addition, we have explored the QAS configuration space to uncover configurations that may have even more attractive properties as reactors. Our exploration led us to the discovery of new classes of configurations and enabled us to demonstrate the richness of the landscape [15].

This paper is organized as follows: In section II we introduce the baseline configuration, for both the basic physics properties and the coil geometry. The physics and coil configurations are used in the systems and engineering studies reported in the companion papers in this issue. In section III we discuss the methodology and approaches we used to develop our configurations. The detailed discussion of the physics basis for the baseline configuration is given in section IV. In section V we present results of a broadened study of the configuration space using two classes of configurations as examples. These advanced configurations have not been examined in detail in the systems and engineering designs but hold the promise that compact stellarators of even more attractive properties as the core of fusion power plants may be found. In section VI

we discuss the R&D needs to resolve some of the design issues that we encountered during the course of the ARIES-CS study. A summary and conclusions are given in section VII.

II. THE BASELINE CONFIGURATION

II.1. Characteristics of the Plasma Configuration

The baseline plasma configuration, N3ARE, selected for detailed systems code and engineering design analyses, is a three field period configuration with a plasma aspect ratio 4.5 and major radius 7.75 m. The aspect ratio is similar to that of NCSX and the configuration may be regarded as an extension or upgrade of NCSX. The major radius is determined primarily by the fusion power and tritium breeding requirements. The fusion power output, P_f, is proportional to $\beta^2 B^4 R^3/A^2$, with the proportionality constant being the normalized, volume-averaged fusion reactivity. Here, B is the magnetic field at the magnetic axis, β is the ratio of the average plasma pressure to the vacuum magnetic pressure, R is the plasma major radius and A is the plasma aspect ratio defined as the ratio of the plasma major radius to the average minor radius around the torus. A steady state is attained when the power outflow is balanced by the power input from the charged fusion products, the α particle in the case of DT fusion. The optimization for COE in the systems code led to the design point characterized by B=5.7 T, $\langle n \rangle = 4.01 \cdot 10^{20}$ m^{-3}, $\langle T \rangle$=6.55 keV, Zeff=1.13 and β=6.4% for a 1 GW electric power plant, where, $\langle n \rangle$ is the average ion density, $\langle T \rangle$ is the density weighted average temperature. Our plasma has a volume 444 m^3 (or equivalently, $0.95 \cdot R^3$), and a surface area 707 m^2 ($11.78 \cdot R^2$). The total fusion power is 2436 MW. The total toroidal plasma

current is estimated to be ~4 MA due to neoclassical bootstrap current. The plasma density is about 1.5 times higher than the Sudo density [16] but it is consistent with recent experimental data [17]. The density is chosen to minimize the energy loss of alpha particles, which is about 5%. The impurity density is chosen to increase the core radiation by introducing Fe (0.008%) to reduce the particle heat load on the divertor. The configuration has a magnetic well of ~1% in the absence of the plasma pressure. The well deepens to ~15% at 5% β. The effective helical ripple (ε_{eff}) of the configuration is very low, ~0.6% at the last closed magnetic surface (LCMS) and ~0.1% in the core region. The effective ripple is not sensitive to the change of the magnitude and profile shape in the plasma pressure. The path to ignition requires a minimum supplemental power of ~20 MW. For discussions of the systems parameters the reader is referred to the companion article on the systems optimization studies [18].

The baseline plasma is a member of the configuration family whose magnetic spectrum has a toroidally quasi-symmetric structure but the residue mirror and helical terms are "biased" to retain a small magnitude, typically a few percent of the magnetic field strength on the axis, to improve the orbit confinement for energetic particles. As noted earlier, QAS allows us to develop configurations with smaller aspect ratios. We find that by introducing the selected non-axially symmetric ($n\neq0$) components in the low aspect ratio QAS the secondary ripple wells, if present, may be modified in such a way that ripple-trapped loss of energetic particles is minimized (Section III.2).

The geometry of the LCMS is illustrated in Fig. 1. In Fig. 2 we show four cross sections of the plasma at toroidal angles 0, $\pi/9$, $2\pi/9$ and $\pi/3$. The presence of the triangular, square and pentagon component in the shape is evident, giving the

configuration a distinctive bullet shaped section at the toroidal angle $\pi/3$. We find that these components are helpful in making the plasma less susceptible to MHD instabilities and at the same time enable the plasma to maintain good quasi-axisymmetry. The shape has the general characteristics of NCSX. Figure 3 shows the contours of magnetic field strength as functions of normalized toroidal and poloidal angles on a flux surface halfway in the radial coordinates of the normalized toroidal flux. These contours show the underlying quasi-axisymmetry of the configuration as the lines are in the toroidal direction in most poloidal angles, but one may also observe deviations from this quasi-symmetry, particularly on the inboard high-field side of the torus, resulting from having the biased residues in the magnetic spectrum.

In Fig. 4 are plots for the eight largest non-axially symmetric components in the magnetic spectrum as functions of the normalized toroidal flux. These residues are small. The mirror term, $B_{m,n}=B_{0,1}$, and the helical component, $B_{1,1}$, are the largest, being ~1-2% of the field strength on the magnetic axis. Here, m and n are the poloidal and toroidal index, respectively. All other components are limited to below 1%. In NCSX, as a comparison, the largest two components are $B_{2,1}$ and $B_{3,2}$, having magnitudes ~2% at the plasma edge, but $B_{0,1}$ and $B_{1,1}$ are vanishingly small. The mirror and helical terms in our baseline configuration, although not large, are sufficient to alter the ripple structure to reduce the loss channels for α particles. An example is shown in Fig. 5 where |B| is followed for five poloidal transits along a field line on the surface at r/a=0.7. We observe that there are large peaks and valleys on the high field side of the field line, but they are not important for the particle loss [19]. In the regions of the main toroidal well the

secondary ripples become less frequent in numbers and for those that do appear they are narrow and shallow.

II.2. Characteristics of the Baseline Coils

The baseline coils are a set of modular coils which provides the main fields to shape the plasma and a set of poloidal field (PF) coils which provides the control of plasma equilibrium in response to pressure changes. A picture showing the modular coils is given in Fig. 6. The modular coils follow the stellarator symmetry, with three different coil shapes for a total of eighteen coils over the three field periods. The coils are designed to be sufficiently far from the last closed magnetic surface to reduce ripples in the plasma due to the discrete coils and to allow rooms for blanket and shielding. One of the most important figures of merit for optimizing stellarator power plant is the so-called coil aspect ratio $A_c=R/\Delta_{min}$(C-P), the ratio of the plasma major radius R to the minimum separation between the center of the coil winding and the last closed magnetic surface Δ_{min} (C-P). Too large a coil aspect ratio may lead to a large power plant because of the required minimum shield/blanket thickness. Too small a ratio may lead to a complicated coil because of the rapid decay of the needed high-order harmonics of the magnetic field. The baseline coils were designed to have a coil aspect ratio 5.9 and also a coil-to-coil separation ratio R/Δ_{min}(C-C) = 10, where Δ_{min}(C-C) is the minimum separation among coils. Thus, for the baseline configuration there is a minimum separation of 0.77 m between adjacent coils and a minimum distance of 1.31 m from LCMS. A plot showing the coil to plasma distance in the entire toroidal-poloidal domain is given in Fig. 7. The distance in the neighborhood of the minimum separation increases sufficiently fast that a

tapered (non-uniform) blanket and shield system may be used to minimize the major radius of the reactor [20].

The maximum magnetic field in the coil is about 3 times the field at the magnetic axis if the conductors had a square cross section with side width 0.3 m (not the reference design). This peak field ratio is reduced to ~2 for square conductors of width 0.6 m. The use of ribbon-like cross section for coils seen in Fig. 6 is our further effort to maximally utilize the space between the plasma and coils for radiation shielding and tritium breeding. The conductors have a height 0.194 m radially and a width 0.743 m toroidally. The maximum field in the winding pack of the coils is ~15 T for an on-axis plasma field of 5.7 T. The high magnetic field in the magnets requires the use of Nb_3Sn as the superconductor material. It is possible to reduce the maximum field by increasing the size of the reactor to yield the same fusion power as it scales like B^4R^3. We allow currents in the coils to be different, 10.8, 13.5, and 13.1 MA, respectively, leading to a maximum winding current density ~94 MA/m^2 and a maximum normalized current $I_c/R\text{-}B = 0.306$ MA/m-T. The lengths of the coils normalized to the major radius are 4.77, 5.08 and 5.14, or 37, 39 and 40 m, respectively, for the three different types of coils. The coils are to be wound in the grooves in a support shell depicted in Fig. 8. In this figure the location and size of the PF coils are also shown. The currents required in these PF coils are estimated to be <5 MA-turns, based on the startup scenarios of NCSX [21].

III. METHODOLOGY FOR DESIGNING PLASMAS AND COILS

III. 1. Physics Design and Optimization

The basic physics properties of a stellarator are determined once the last closed magnetic surface is prescribed. As mentioned before, the drift orbit of particles depends only on the magnitude of the field strength, not the vector components. The shape of the plasma may be entirely non-symmetric but the underlying field strength still can be made to follow certain symmetry. The residues in the magnetic spectrum due to the plasma shaping to give perfect symmetry cannot be entirely eliminated in the entire volume of the plasma; only approximate quasi-symmetry can be achieved in practical designs. The physics optimization then is such that the plasma boundary is allowed to deform to maximize the symmetry property in the plasma while constraints are imposed to improve other physics properties. Mathematically, this is a non-linear, constrained optimization problem.

It is convenient to represent the boundary of plasma in the following compact form:

$$R + iZ = e^{iu} \sum \Delta_{m,n} e^{-imu+inv} \qquad (1)$$

where R and Z are the radial and axial components of a cylindrical coordinate, m and n are the poloidal and toroidal mode numbers, u and v are the normalized poloidal and toroidal angle-like variables [22]. The coefficient $\Delta_{1.0}$ is the plasma major radius and $\Delta_{0,0}$ is a measure of the plasma minor radius. Without losing generality, we let $\Delta_{0,0}$ be 1 so that $\Delta_{1.0}$~A. For the m=1, 2 and 3 terms in (1) we obtain helical excursion, elongation and triangularity, respectively, in the shape of the plasma. For m=-1 we obtain the crescent that contributes to the magnetic well and helps with stability. Most of the

rotational transform in our cases comes from $\Delta_{2,1}$. The magnetic field strength on an equilibrium surface, s, is typically represented as a double Fourier series in Boozer magnetic coordinates,

$$B(s) = \sum B_{m,n}(s)\cos(m\theta - [n - \iota m]\phi) \qquad (2)$$

The coefficients $B_{m,n}$ in (2) for the poloidal mode number m and toroidal mode number n are typically referred to as the magnetic spectrum. In (2), ι is the rotational transform on a surface labeled by the normalized toroidal flux s and $[n-\iota m]$ denotes this being the straight field line coordinate. For quasi-axisymmetry, one minimizes contributions of $B_{m,n}$ for which n≠0. Although $\Delta_{2,1}$ delivers most of the rotational transform in our cases, the corresponding term $B_{2,1}$ in the spectrum is usually small.

For the baseline plasma, the last closed magnetic surface is characterized by $\Delta_{2,1}$=-0.41, $\Delta_{2,0}$=-0.25, $\Delta_{-1,-1}$=0.17, $\Delta_{3,1}$=0.15, $\Delta_{3,0}$=0.14, $\Delta_{-1,0}$=0.11, $\Delta_{0,1}$=0.07, $\Delta_{3,2}$=0.06 and $\Delta_{4,0}$=-0.06, giving an average elongation ~1.7 and triangularity ~1.

We began the development of our configurations by restricting m≤6 and n≤4 in the initial prescription for the plasma boundary. An initial set of $\Delta_{m,n}$ was chosen and solutions were sought such that residues in the magnetic spectrum, with the exception of a few selected components, were minimized and the following conditions were met. We require that the residues in the magnetic spectrum be low enough so that the effective helical ripples on all surfaces will be < 1% and that the collisionless loss orbits of alpha particles are minimized during a small number of toroidal transits, typical ~500. The complete calculation, including the slowing down processes, for α loss is carried out during the analysis phase as such a calculation is too expensive to be practical in optimization. We asked, moreover, that the rotational transform supplied by rippling the

boundary alone be of certain shape and magnitude (for the baseline, monotonically increasing and of magnitude 0.45), that the transform increases as radius increases, and that there exists a magnetic well in the absence of the plasma pressure. Although recent results from W7AS and LHD showed that the linear, ideal MHD theories have limited applicability in predicting the stability limit in stellarators, we still included the stability to the infinite-n ballooning and ideal external kink modes calculated based on such theories as constraints in the optimization since in the NCSX studies we found that including, for instance, the external kinks as a constraint the structure of local shears would respond in such a way that the resulting configuration would generally have more favorable MHD stability characteristics [23]. However, we did not strictly enforce such constraints and in some advanced configurations these constraints were relaxed considerably, as suggested by the nonlinear theory [24]. Additionally, we monitor the boundary harmonics to minimize the impact of resonant perturbations due to the existence of low order rational surfaces. These perturbations manifest in the formation of magnetic islands, which, if large enough, would enhance the radial loss due to plasma flow along field lines.

The search and optimization were carried out by an efficient non-linear optimization package, STELLOPT, developed during the design of NCSX [25]. In this package either a modified Levenberg-Marquadt algorithm or the genetic or differential evolution techniques may be used for the search. VMEC [26] is used for the equilibrium evaluation. Function evaluations were made in parallel, in either the gradient calculations when the local gradient search algorithm is used or the “fitness” calculations when the genetic or differential evolution algorithm is used. We find that it is also useful to study

plasma equilibrium by the NSTAB code [22, 27] and the PIES code [28]. The PIES code is useful when used to examine the quality of equilibrium since it does not presume the existence of nested flux surfaces. The optimization program uses separate modules to evaluate elements of the penalty function. These modules include evaluation of parameters concerning the basic plasma properties (such as the desired amount of external rotational transform, the magnetic shear, magnetic well depth), the MHD instability growth rate (such as external kinks, infinite-n ballooning), and transport figures-of-merit (such as ε_{eff}, diffusion coefficients, collisionless loss of α particles). Typically, we evaluate the effective helical ripple by NEO [29], the α-particle transport by the guiding center code ORBIT3D [30], the kink stability by Terpsichore [31], the ballooning stability by CORBA [32] and the thermal transport by TRANS [33].

The importance of α loss resulting from the breaking of axisymmetry in DT stellarator reactors has been realized for quite some times. Gori et al. have used a Monte Carlo algorithm to minimize the loss of trapped alphas [34]. Subbotin et al. have tried the method of maximizing the psuedo-symmetry and the technique of closing the contours of the second adiabatic invariant [35]. We have examined various methods and find that a combination of minimizing the residues of the non-axisymmetric components in the magnetic spectrum and maximizing the average resident times of the collisionless α's of all classes provides a robust and efficient means to identify configurations with the reduced α loss. In applying the ORBIT3D Monte Carlo code to the physics optimization that involves only the collionless process, the parameters that would be affected by the "randomness" are only the initial positions and pitch angles of the particles. By using the same seed to start the pseudo-random number generator in the Monte Carlo process, the

random walks would be highly correlated in the gradient calculations and the resulting stochastic effect is minimized in the determination of the direction of the steepest descent in the equilibrium parameter space. We find that the Monte Carlo approach is effective and robust even when restricted to a small sample size, a small cutoff lost fraction and a limited number of toroidal transits.

It is important to point out that, unlike other ARIES studies for tokamaks where ample theoretical and experimental understanding have been used to extrapolate to the design of reactors, there is very little data for drift-orbit optimized stellarator devices. The understanding of plasmas in three dimensional configurations is from non-drift optimized devices. Experimental data from existing devices indicates that stellarators are more resilient to MHD perturbations than the linear, ideal theory tells us. The widely used ISS95 scaling [36] for the energy confinement times was derived from a set of small stellarators, most of them not drift-optimized. Results of recent experiments have already exceeded the prediction by this scaling law and a scalar "H" factor is typically applied to match the increased confinement observed in experiments. The Sudo density limit [16], which was derived from an earlier heliotron and which has been considered to be more appropriate for stellarators, has been exceeded (e.g. in LHD [17]). Perhaps the nonlinear theory will help to address these issues [33, 45]. At present, there are uncertainties in setting up the physics targets in the design of optimal configurations. The approach taken here is generally conservative (imposing more constraints) and may be relaxed when further understanding is available, e.g. from NCSX experiments.

III.2. Coil Design and Optimization

Coils that produce the designed target plasma shape may be constructed by requiring that the surface normal component of the magnetic field they produce on the LCMS cancels that due to the plasma current. Various numerical techniques have been devised for this "reverse engineering" of the coils [37, 38]. We have established a three-staged approach. First, the current potential on a prescribed coil winding surface is determined by minimizing the residues of the magnetic field normal to the LCMS. From the current potential we obtain an approximate coil design. Second, we allow the winding surface geometry as well as the geometry of the coils wound on this surface to vary so as to not only minimize the field errors on the last closed magnetic surface but also enforce additional constraints, such as the minimum separation to the plasma or to the neighboring coils, coil curvature and other engineering properties. We typically require that the maximum local residue ($|\delta B_n|/B$) be <2% and the overall average residue be <0.5%. Lastly, we directly solve for the free boundary equilibrium and optimize both the physics and engineering properties simultaneously instead of minimizing the normal field errors on the boundary defined by the original fixed boundary plasma, again by allowing both the winding surface topology and the coil geometry to vary, using coil parameters obtained from step 2 as the initial condition. The last step is a complicated and difficult procedure and has been used here only for the very low aspect ratio MHH2 case (see Section V.1).

We represent the coil shapes parametrically as two-dimensional Fourier series in terms of toroidal and poloidal angles on a winding surface. The winding surface itself in turn is represented as Fourier series in the toroidal and poloidal angles. This double

representation has an advantage in that it allows one to choose the initial coil geometry in a more flexible and intuitive way. The initial choice of the winding surface is important since the optimization is highly non-linear and the configuration space is complex with many valleys and hills. The optimization finds a "local" minimum of the penalty function we specified. We cannot ascertain the existence of a unique solution in this multi-dimensional optimization.

In DT reactors, the requirements of tritium breeding and coil protection from radiation damage typically set the minimum thickness for the blanket and shielding. As mentioned before, if the coil aspect ratio, A_c, becomes too small, allowing more room for the first wall, blanket and shielding for a given R, the shape of the coils may become too complex to be attractive. If the ratio becomes too large, the size of the machine may have to be increased to provide enough space and therefore the machine may become too big and the power density too low, irrespective of the compactness of the plasma itself. In addition, the maximum magnetic field in the plasma, and therefore the power density, is limited by the maximum allowable field in the coil body. Figure 9 shows an example study of the peak magnetic field in the coils as the coil aspect ratio is varied in one of our earlier studies for the baseline configuration. It is seen that there is a critical coil aspect ratio about 6. Below this, the increased coil current and coil complexity lead to higher fields in the coil body. Above this, the increase in current density due to the limited space for the coil also leads to higher fields. We therefore included the coil aspect ratio as a constraint in the design optimization.

Additionally, coils must also have adequate separations among themselves and have sufficiently large bend radii throughout the winding. These considerations will help

coil manufacturing, port installation, machine assembly and remote maintenance. Thus, we also impose the constraints of coil separation ratio and the minimum radius of curvature in the coil optimization. We allow coils to have different currents, but they have to maintain the stellarator symmetry (i.e. $R(\theta,\phi)=R(-\theta,-\phi)$, $Z(\theta,\phi)=-Z(-\theta,-\phi)$). Typically we search for solutions with coil aspect ratio <6, coil separation ratio < 12, and the ratio of the major radius to the minimum radius of curvature <12. During the third stage of optimization in which free boundary equilibrium is solved, we vary coil geometry as well as coil currents to minimize the non-axisymmetric "noise", the effective ripple, the collisionless loss of α particles, etc., as discussed in III.1.

IV. PHYSICS BASIS FOR THE BASELINE CONFIGURATION

IV.1. Plasma Equilibrium and MHD Stability

Equilibria of the baseline configuration have been studied using both the VMEC and PIES codes for β ranging from 4% to 8%. In VMEC, it is assumed that flux surfaces are closed and nested. Most of our stability and transport calculations take advantage of this assumption to map VMEC solutions to the Boozer magnetic coordinates for analysis. In Fig. 10 are flux contours at the oblate cross section calculated using VMEC for an equilibrium at 5% β. The profiles of plasma pressure and current used in the calculation are illustrated in Fig. 11. The normalized plasma current (Ip/R-B) due entirely to bootstrap at β=5% is ~0.08 MA/m-T and it is proportional to ~β/ι, where ι is the total rotational transform. The bootstrap current is determined by the Fourier spectrum of |B| in Boozer coordinates. In QAS, the $n\neq0$ coefficients are small and the bootstrap current is similar to that in a tokamak. In particular the bootstrap current is in a direction that

reinforces the externally generated rotation transform. Here, we adopted, as a starting point, the pressure and current profiles from ARIS-RS [39], in which the current profile was well aligned with the bootstrap current. Because the bootstrap current is determined by the n=0 components of |B|, we retain rough consistency with the bootstrap drive. Adjustments were made in the profile using a three-dimensional bootstrap code [40] in which a connection formula valid in the entire range of collisionality was used in the calculation of the bootstrap current. The rotational transform profile as a function of the normalized toroidal flux for β~5% is given in Fig. 12 in which both the external transform and the total transform including the internal contribution from the plasma current are shown. The external transform ranges from ~0.4 to ~0.5, and the total transform rises to ~0.7 near the edge. The core transform is large enough such that the Shafranov shift ($\sim\beta A/\iota^2$) is modest, ~10% of the minor radius at 5% β.

Figure 13 shows the result of an equilibrium calculation using the PIES code which does not presuppose the existence of nested flux surfaces. Field lines are followed to trace out the separatrix near rational surfaces. It is seen that although the total rotational transform passes through the 3/5 and 3/6 resonance, the surfaces maintain an overall good integrity throughout the entire plasma with only a relatively small loss of the fluxes. Indeed, the resonance perturbation to the 3/5 mode is very small so that this island chain is not clearly resolved in the calculation. The shear in our configuration is designed to have positive sign relative to the direction of the plasma current, therefore the perturbed bootstrap currents suppress magnetic island when a resonance exists. This effect is not included in the PIES calculation. In NCSX, an estimate of this effect was made and it was found that, when 50% of the rotational transform is from the bootstrap

current, an island whose width would otherwise be 10% of the minor radius is suppressed to about 0.5% of the minor radius [41].

We have used computer codes based on the linear, ideal MHD assumption to monitor the stability properties of our configuration and to help guide the design optimization. However, we should point out that, although the upper linear MHD stability boundaries for β were found to be $\leq$2% in LHD and W7AS, experiments achieved beta greater than 3-4% for durations much longer than the energy confinement time (for example, see [42]). A non-linear analysis for one of our earlier QAS configurations also indicated a higher stability boundary than that calculated by the linear, ideal MHD [24]. Nevertheless, codes based on the linear, ideal theory are readily available, easier to use and do not demand too much computational resources. We use them to delineate the linear stability boundary and as a basis for discussing MHD stability characteristics, but we do not restrict beta in the search for the operating point in the systems optimization since the credible MHD beta limit is not known at present. Beta limits in stellarators are an important research subject that needs to be systematically studied in the years to come. We have targeted 4% linear stability beta in the configuration optimization, similar to that used in developing the configuration for NCSX. The beta chosen for the baseline operating point is ~6.5%, or about 60% above the targeted linear stability boundary.

Our analysis showed that the configuration is stable to the vertical mode, as expected from the theoretical analysis [43]. The control coils normally required in tokamaks are not needed. The Terpsichore code [31] is used to study the kink stability. The calculation based on the resolution used in the optimization process (49 radial grids, 59 equilibium modes, 264 Boozer modes, 91 perturbation modes) indicates that the kink

stability boundary of the configuration is about 4%. At 5% β, the configuration is weakly unstable without a conducting wall. A systematic sensitivity study for the configuration using 197 surfaces and up to 101 toroidal-poloidal angle combinations yields a slightly more pessimistic but more complete picture. Preliminary results with the higher resolution indicate the reference case with β = 4.06% is actually slightly unstable. The "symmetry preserving" (i.e. n = 3 family) mode is a predominantly m/n = 9/6 mode strongly peaked at the edge with 5/3 and 10/6 sidebands and is near marginal (eigenvalue equal to the square of the growth rate in Alfven time units of $\gamma^2 \sim 10^{-6}$). However, the symmetry breaking mode is a much more global m/n = 3/2 mode with 6/4, 2/1, 2/4, and 8/5 sidebands. The growth rate, with $\gamma^2 \sim 10^{-4}$, is moderately small indicating a proximity to the β limit. The β limit found from varying the pressure uniformly at fixed ι then appears to be a little below β = 4%. Further convergence studies would be needed to fully confirm this but the LHD and W7-AS experimental results seem to indicate that this level of instability at β = 4% is robustly tolerated in practice. At higher β, several modes become unstable and for β = 8.2% there are two external and one internal symmetry breaking modes unstable with one unstable symmetry-preserving mode. For the most unstable symmetry-breaking mode, the 2/1 component is dominant. The external "symmetry-preserving" and symmetry-breaking modes are stabilized by a conformal wall at 1.2 times the average plasma minor radius. However, the internal symmetry breaking 2/1 mode remains unstable even with the wall on the plasma boundary, albeit with a very low growth rate, $\gamma^2 \sim 10^{-7}$. This is not expected to be significant.

The reference equilibrium has an ι = 2/3 surface right at the edge of the plasma and the sensitivity to the presence of this ι = 2/3 surface was also investigated. With the

2/3 surface removed at constant β, the equilibrium is marginally unstable to an m/n = 13/5 mode peaked in the core. On increasing ι so that the ι = 2/3 surface moves deeper into the plasma, the 3/2 mode is destabilized. This mode requires a conformal wall within 1.1 times the average plasma minor radius for stability.

The study for the Mercier mode showed that the configuration is stable at 6% β and for the infinite-n ballooning modes stable at ~4% β. At 5% β, however, the ballooning unstable zone occupies only ~10% of the radial width peaked at r/a~0.9. In NCSX, it was found that using the finite but high-n calculation (n~20) to account for the finite Larmor radius effect results in a much higher ballooning beta limit, typically by ~50% [44]. Because of the similarity of the field structure between NCSX and the baseline plasma, we believe that our configuration is actually stable against the ballooning modes to ~6% β. We have observed the beneficiary effect of the mirror term $B_{0,1}$ on the ballooning stability in our previous study of a three-field period QAS [24]. We are able to take advantage of the mirror field in the baseline configuration to improve both the stability and confinement of the fast particles.

The rotational transform has a positive shear in most of the plasma region, thus the configuration is expected to be stable to the neo-classical tearing modes as well. The 6/9 resonance and the shear reversal near the boundary are of concern. We shall investigate the need to modify the transform profile in the future.

Plasma equilibria depend upon the details of the plasma pressure and current profiles. Sensitivity calculations have been carried out to study their effects on the quasi-axisymmetry and MHD stabilities. The pressure profile was represented as $(1-s^a)^b$ in this study with a varied from 1 to 10 and b from 1 to 2.5. Here s is the normalized toroidal

flux. The corresponding current profiles were derived, with additional variations in the density profile, from calculations of a 3-dimensional bootstrap code [39]. We find that quasi-axisymmetry is largely unaffected by changes in the pressure or current profiles since most of the rotational transform is generated externally by the shaping of the plasma. The MHD stability responds more favorably when the peak of the current density shifts outward (resulting in a larger global magnetic shear). Figure 14 shows a current profile used in one of our sensitivity studies. It is quite different from the one used in the baseline plasma and is less favorable with respect to the stability as understood from the linear, ideal MHD. Figure 15 shows the amount of boundary deformation relative to that of the baseline configuration needed to completely stabilize the external kink instability at 5% β in the limit of the linear, ideal MHD theory. The fact that the needed modification is so small for the very different current profile indicates that the configuration indeed has a favorable MHD stability characteristic. Based on our sensitivity studies and in light of the results from recent experiments, we believe that the choice of ~6.5% β for the operating point is reasonable from the standpoint of MHD stability. If the plasma in this configuration turns out to be more stable than the linear calculation indicated, either from non-linear analyses or from experiments, then some relaxation of the shaping constraint may become possible, which may lead to less complex coils. If, on the other hand, the selected operating β turns out to be too high, it is possible, for example, to increase the major radius to ~8.25 m to bring β down to ~4% with only ~7% penalty to the COE [18].

IV.2. Particle Transport and Confinement

As discussed earlier, the magnetic field structure, although mostly quasi-axially symmetric, has certain distinctive features in the spectrum. In a QAS configuration, the connection length is long between good and bad curvature regions so that particle transport is sensitive to the distribution of secondary ripple wells along the field lines. The small but non-negligible mirror term, $B_{0,1}$, together with the side-band helical term, $B_{1,1}$, reduce the effects of the secondary wells along the path of the toroidally trapped particles, thereby reducing transport losses, as confirmed by a detailed analysis of the Bx∇B drifts [19]. The secondary wells are either shallow or closer to either inboard or outboard side of the field line where particles with turning points inside the ripple wells average over smaller gradient drifts. We note that, because we can only achieve quasi-symmetry, the secondary ripple wells will be present. However, it is possible to preferentially select or bias the components in the magnetic spectrum to reduce the harm caused by them. In our baseline configuration the effective helical ripple is very small. Shown in Fig. 16 is the dependence of the effective ripple on the plasma radius for β~5%. We observe that the effective ripple, ε_{eff}, is less than 0.1% in the core of the plasma and the maximum value is <0.6%. The diffusion coefficient for the collisionless transport is proportional to $\varepsilon_{\text{eff}}^{1.5}$ so that we expect the loss due to the neo-classical transport will be small when compared to the anomalous. The effective ripple does not change much as β varies. The energy confinement time required for power balance at steady state is ~1 s. Using the stellarator ISS95 scaling [36],

$$\tau(s) = 0.256 a_m^{2.21} R_m^{0.65} P_{MW}^{-0.59} n_{20}^{0.51} B_T^{0.83} \iota^{0.4} \qquad (3)$$

one finds that this requirement will be met if we allow an "H" factor of ~2 in the scaling. This enhancement factor has been achieved in experiments. Monte Carlo simulations

have been employed to verify some of our conclusions [45]. We further note that the recently updated ISS04 scaling [46] will give a more favorable confinement. The analysis of the 2004 international stellarator data base suggests that lower values of effective helical ripple may correlate to the higher values of confinement improvement. Our configuration is designed to have very low effective ripples, being ~0.05% at r/a=2/3.

In addition to the thermal transport, the loss of alpha particles is an important issue not only because it affects the power balance but also because it drives the divertor and protective plate design. The configuration is designed to minimize the collisionless loss by optimizing the secondary ripple well distribution. It is also optimized to reduce the collisional loss by increasing the collisionality of the alpha particles with the background thermal species. Generally, we find that the alpha energy loss scales like R^2B^2 for a fixed plasma aspect ratio. The loss also scales strongly with respect to the collisionality. Figure 17 shows parametrically the effects of the collisionality on the loss of alpha in two reactor sizes. The high collisionality reduces the alpha particle slowing down time. This also decreases the total energy in the alpha particle distribution function, decreasing the drive for fast ion and Alfvenic instabilities. In this parametric study both the temperature and density profiles of the background ions and electrons were assumed to be parabolic and the α emission profile of the form $(1-r/a)^8$. In the baseline configuration, we have chosen a high density and high magnetic field intensity for the plasma to minimize the loss, but they are consistent with both the density limit experimentally observed and the critical field in the superconductor at the designed current density. Our analysis shows that the loss fraction of the energy of alpha particles is ~5%, or ~20 MW. This result is based on the ORBIT3D Monte Carlo calculations in

which 4096 alphas were followed for ~200 ms, or about twice the slowing down time, with an estimated statistical error of ~15%. In addition to the parabolic profiles used in the parametric study, in the final analysis we have also carried out a calculation using a hollow density profile similar to that used in the systems study [18] and a temperature profile that, when combined with the hollow density profile, would yield a pressure profile similar to that used for the equilibrium and stability studies. All these calculations showed similar losses within the statistical error.

The footprint of the alpha particles leaving the last closed magnetic surface is illustrated in Fig. 18, and the energy distribution of these lost particles is further graphed in Fig. 19. There is a distinctive band structure in both the toroidal and poloidal angles as the alphas left the last closed magnetic surface. The exact fate of the lost particles has yet to be studied. If we assume that the high energy particles directly hit the first wall, the average heat load would be ~0.2 MW/m^2, although the peak heat load due to the localization of the loss could amount to a couple of MW/m^2. Given that the allowable total heat load on the first wall could be designed to ~10 MW/m^2, the additional power due to the lost α may be tolerable if a proper design is taken. Of more importance, perhaps, is the damage to the properties of the wall material caused by the implanted particles. If, on the other hand, we assume that all lost particles end up on the divertor plate, the heat load on the divertor, which is ~1% of the fusion power, would be about the same as the load due to the conduction loss of the thermal particles if a radiation fraction of 0.75 is used for both the core and the plasma edge at steady state, see the power flow in Ref. [18].

IV.3. Magnetic Topology for Edge Modeling

We have studied the magnetic topology in the boundary region by the use of the MFBE code which was developed for W7X and has been modified to take into account the presence of plasma current [47]. Magnetic fields from coils are calculated using the Biot-Savart law and fields due to plasma current are evaluated using the "virtual casing" principle. In Fig. 20 we present two Poincaré plots at the toroidal planes of the crescent and oblate cross sections for the MFBE solution of a representative calculation. In this calculation, field lines launched at mid-plane from radial positions both inside LCMS and outside LCMS to a distance of 0.01 m on the outboard side were followed for 200 toroidal revolutions or until they left the "computational box". The location of LCMS is self-consistently determined by comparing the MFBE and VMEC generated equilibrium. It is seen that the field lines are not entirely ergodic as the puncture points are not randomized. There is an appreciable flux expansion at the crescent shaped section. The expansion is still large even at 30 degrees from this section. Localized divertors may be designed in the regions of the strong flux expansion. We have used the balance of energy and momentum in conjunction with a two-point model to relate the connection length to the up- and down-stream temperatures and densities. Additionally, we have used the carbon impurity to match the radiative fraction assumed in the divertor region in the systems analysis [18]. The model is similar to that used by Borrass for ASDEX [48]. The result suggests that an operational window exists even for the short connection lengths. The divertor radiation fraction sets an upper limit on the downstream temperature, which is typically ~5-20 eV. It was found that for parameters of the baseline design the required connection length is ~100 m for the separatrix temperature T_s~200 eV and

density $n_s \sim 8 \cdot 10^{19}$ m^{-3}, ~500 m for T_s~400 eV, $n_s \sim 6 \cdot 10^{19}$ m^{-3} and ~2 km for T_s~800 eV, $n_s \sim 5 \cdot 10^{19}$ m^{-3} [49]. We found that, if divertor plates were placed at ~0.2 m from the last closed magnetic surface near the tip of the crescent-shaped section, an average connection length of ~300 m could be "designed". The characteristics of the connection length distribution obviously depend on the toroidal and poloidal widths as well as the shape of the divertor plate. The divertor design is discussed in the companion paper [50] where efforts were made to maximize the wetted area and to minimize the angle of incidence to reduce the peak heat load.

V. EXPLORING CONFIGURATION SPACE FOR OTHER POTENTIAL CANDIDATES

The baseline configuration belongs to a family whose members all have similar magnetic field topology with their aspect ratios in the range 4 to 6 and their average externally generated rotational transforms taking the value 0.45 or 0.65. The magnitude of the mirror $B_{0,1}$ is as high as ~5% for A~4 configurations but it drops to essentially zero as A approaches 6. The discovery of the existence of a family, not just a single configuration, reveals the richness of the QA configuration space. Indeed, the baseline family was developed as part of our efforts to survey and study the landscape with respect to the aspect ratios, number of field periods and rotational transforms. In this section we discuss some additional configurations of different families that may also be of interest insofar as designing compact stellarator power plants is concerned.

V.1. Configurations with Very Compact Plasmas and Coils

In the family of the baseline configuration, the smallest aspect ratio such that the plasma still maintains acceptable quasi-axisymmetry (section III.1) is ~1.3 per field period. For two field periods, this means that reactors having an aspect ratio as low as 2.5 may be designed. The search for this low aspect ratio plasma with simplified shapes to reduce the coil complexity has led to the development of new configurations in the family generally known as MHH2 [7, 45]. We emphasize in this search the less complex coils because the attractiveness of low aspect ratio configurations as compact, small-sized reactors can only be realized if coils can also be designed with sufficient compactness and with good engineering properties. To this end, the design for MHH2 configurations has benefited from the relaxation of the adherence to the linear, ideal MHD stability constraint, making shapes of the plasmas and coils simpler and smoother. The non-linear theory has been applied instead [22, 27, 33]. We note that the basis for relaxing the linear, ideal MHD stability constraint is enhanced by evidence gathered from recent experiments [1, 2]. Theoretical results from using the non-linear, perturbed equilibrium approach in NSTAB [27] indicate that the low aspect ratio MHH2 configurations are generally stable to MHD perturbations at a reasonably high beta, typically ~5% [45].

In Fig. 21 we illustrate the cross sections of a configuration, MHH2-K14, for which modular coils have been carefully designed using the entire three-staged approach discussed in III.2. A top view of the modular coils is also presented in Fig. 21. There are four distinctive types of coils in each half period for a total of 16 coils in two field periods. The winding surface was constructed in such a way that the outboard distance from the last closed magnetic surface was twice the inboard distance to minimize ripples in the plasma due to the effects of discrete coils. The coils are designed such that the coil

aspect ratio is 5.5 and the coil separation ratio is 10. The ratio of the plasma major radius to the minimum coil bend radius is ~13. The coil aspect ratio is about 10% smaller than that of the baseline configuration. Also, the plasma-coil separation changes more slowly compared to the baseline in both the toroidal and poloidal directions in the neighborhood of the minimum separation. The geometry is therefore more suitable for the implementation of a uniform blanket and shield. The maximum field strength in the coil body is ~3 when normalized to the field on the magnetic axis for 0.4x0.4 m^2 conductors and the maximum current in the coils is 0.316 MA/m-T when normalized to the plasma major radius and the on-axis magnetic field. Analyses based on equilibria calculated by VMEC showed that the effective helical ripples are less than 0.8% in the entire plasma of MHH2-K14 and that the energy loss fraction of α particles in a reactor with R=7.5 m and β=5% is ~4%. The eight largest non-axially symmetric components in the magnetic spectrum are shown in Fig. 22. The most prominent component is again $B_{0,1}$, with all others having magnitude less than 1%. The configuration also has a notable magnetic well, ~3.6%, in the absence of the plasma pressure.

Thus, we have shown that compact coils with good engineering properties can be constructed for very low aspect ratio very compact QAS configurations. To further increase the compactness will require the coil aspect ratio be further reduced, which is not easy to do. We were able to develop a version of the coils in which the coil aspect ratio was further reduced by 10%, to ~5, but the physics properties of the resulting plasma still need some improvement. Additionally, the rotational transform passes through the ι=2/4 surface so that large m=4 islands could appear. Ways to minimize such

resonant perturbations are under investigation in order to assure the integrity of the flux surfaces.

V.2. Configurations with Low Magnetic Shear

The integrity of equilibrium flux surfaces and the MHD stability determine the attainable beta of a stellarator configuration. There are indications from PIES analyses for W7AS that a stochastic region appears at the plasma edge when the magnitude of β exceeds a threshold value and the stochastic region broadens as β increases, resulting from the strong local compression and distortion produced by the Shafranov shift [51]. In QAS configurations, the bootstrap currents may give rise to rotational transform with large shears. A large magnetic shear increases the likelihood of introducing more low-order resonances. A large shear also draws rational surfaces closer to each other. Although magnetic islands may be healed by the kinetic effects of the bootstrap current, the possibility of their presence is generally undesirable in the stellarator design as the quality of the flux surfaces could be compromised. To make flux surfaces robust at high beta, one could design the shape of the externally generated rotational transform profile to compensate for the high magnetic shear in the internal transform due to the bootstrap currents to avoid the presence of the low order rational surfaces. We have devised such configurations both for the family of the baseline configuration and for another family, SNS, which is characterized by having large negative shear in the externally generated rotational transform. The finite β rotational transform in these configurations has a small but positive shear.

Figure 23 shows the geometry of LCMS of a three field-period configuration, N3ASDE, of the baseline configuration family whose total rotational transform lies in the region between the 3/5 and 3/4 resonance gap, as shown in Fig. 24. A Poincaré plot at the triangular cross section for an equilibrium solution of PIES at 5% β is given in Fig. 25, where we see that the quality of the flux surfaces is excellent, as expected. The configuration also has good quasi-axisymmetry. The effective ripple is ~0.5% at LCMS and it is much lower in the core. The energy loss fraction of alpha particles is < 5% for reactors with R~8 m. Moreover, the configuration has a magnetic well ~2% in the absence of the plasma pressure and it is stable to the external kinks at ~5% beta without a conducting wall even in the linear, ideal MHD limit. In this configuration, therefore, we have demonstrated that a specially tailored rotational transform as large as 0.23 per field period can be implemented with good particle confinement and MHD stability, although clearly the plasma is deformed more strongly, which may lead to more convoluted coils. Coil design for this configuration has not been attempted.

In Fig. 26 we show another configuration, KJC167, of the SNS family, which has an aspect ratio 6 and whose rotational transform is designed to be between the 3/5 and 3/6 resonance gap at 6% β, as illustrated in Fig. 27. The external transform has a large negative slope to cancel out the effects of the large bootstrap current. In developing this configuration the MHD stability constraint was relaxed in an effort to make the shape less complex. Again, the quality of the flux surfaces is excellent, as seen in Fig. 28. It has superb quasi-axisymmetry as well, with ε_{eff}<0.5% everywhere, and a magnetic well ~4% in the absence of the plasma pressure.

Because of the stronger deformation of the plasma surface, coil designs for these configurations become more challenging. Additionally, for configurations having a large negative shear in the externally generated transform, such as KJC167, we must demonstrate that coils can be designed with sufficient flexibility such that the total transform will be able to skirt low order resonances throughout the entire discharge, not just at the operating point. A preliminary coil design for KJC167 at 6% β is illustrated in Fig. 29. In general, however, coil design and optimization for these configurations remain to be an incomplete and unfinished task.

VI. PHYSICS DESIGN ISSUES AND R&D NEEDS

The physics properties of a compact stellarator reactor and the complexity of its coils are affected by how we optimize the configuration. The optimization requires setting constraints and objective functions. While we have attempted to establish a reasonable set of targets and constraints in the configuration optimization, there are uncertainties as to how much weight we should give to them. These uncertainties can be resolved by experiments and by the advancement of theories. It is the objective of the ARIES-CS study to identify R&D issues that the near term experiments may be able to address. Here we discuss some aspects of the design issue and the R&D needs.

VI.1. α loss and Control of Strike Points

While much has yet to be understood of the confinement of energetic particles in QAS, in a reactor it is important to minimize their impact on the plasma facing components. We need to address the question of whether low alpha loss can be achieved and if alpha loss due to MHD instabilities can be mitigated by operations at high

densities. Furthermore, lost particles near the birth energy may not follow the diverted field lines since the drift velocity and the large Larmor radius may force the escaped particles to lodge in localized areas on the first wall. Understanding the loss pattern and footprint is thus equally important.

VI.2. Stability and Equilibrium Beta

We need to understand beta limiting mechanisms and translate the understanding into a set of measures for the configuration optimization. We need to investigate if $\beta>5\%$ can be achieved and sustained with good confinement and if the pressure driven islands and stochasticity surface can be avoided in the confinement region.

VI.3. Energy Confinement and Scaling

We have used the ISS95 confinement scaling for the power balance. The scaling (and other scaling laws for stellarators as well) was derived based on machines of small sizes without the drift orbit optimization. Clearly, we need R&D to systematically characterize the confinement scaling with respect to parameters important for quasi-symmetric configurations, and see that good confinement is maintained at $\beta>5\%$. Perhaps the Monte Carlo method could be applied more effectively.

VI.4. Operational Limits

We need to understand the limit to the density and controllable core radiation fraction and the conditions under which the plasma purity and low ash accumulation can be achieved. We need to investigate how the density and pressure profile shape depend on configuration and plasma parameters. Typically we assume certain profile shapes in the configuration development. We need to investigate if these profiles can be practically

produced, whether other more optimal profiles exist, and whether the operational limits are sensitive to the profiles..

VI.5. Startup and Control

From power balance and POPCON studies we find that for the baseline configuration the pass to ignition requires a minimum of ~20 MW auxiliary heating power [18]. We need to identify a robust discharge scenario that, while navigating the temperature-density space along the path of the minimum power, would minimize any deleterious impact of low order rational surfaces as the bootstrap current builds up and changes the rotational transform. Presumably, such startup scenarios can be developed in NCSX since the characteristics of the baseline configuration are in many respects similar. Perhaps more importantly, the adequacy of the coils to accommodate startup scenarios needs to be ascertained. We have designed a set of PF coils for the control of the plasma equilibrium. Whether these can be simplified, or other types of coils will be needed, e.g. TF or trim coils, will become clearer once we gain more experience and knowledge as NCSX is commissioned.

VI.6. Coil Complexity

We need to examine whether physics requirements can be relaxed, such as the external transform, the MHD stability, flux surface quality and the amount of ripples in the configuration optimization for the coils. We know, for instance, that the linear, ideal MHD theory does not fully tell the story of stellarator stabilities and that the kinetic effects should heal magnetic islands, but we need to formulate all the important physics into a set of quantitative guidelines so that we will be able to properly take them into account in the configuration development without over-constraining the optimization

process. And clearly, there is also a need to clarify the sensitivity of the critical parameters to the coil design tolerances.

In addition, the coil designs considered so far have not targeted reactor specific issues, particularly maintenance of the blanket and shield inside the coils. Future design studies should explore optimizing the coils to provide large aperture rectangular access to the internal components, to maximize the unit size of the replaceable internal components.

VII. SUMMARY AND CONCLUSIONS

We have explored regions in the configuration space that have quasi-axisymmetric properties and developed configurations that meet the requirements to be the core of compact fusion power plants. These configurations have small aspect ratios and they have been demonstrated numerically to have high equilibrium and MHD stability beta and good confinement for both thermal and energetic particles. We have designed coils for many of these configurations to show that compact coil systems exist that are able to produce plasmas of the desirable quality. The particular configuration selected as the baseline for detailed power plant studies has three periods with a plasma aspect ratio 4.5 and consists of 18 modular coils with a coil aspect ratio 5.9, leading to a design of R=7.75 m for the 1 GW(e) reactor.

The baseline plasma is a member of the family with a biased magnetic spectrum. This family of configurations possesses attractive physics properties for the design of compact stellarator power plants. The potential of many of the configurations in this family has yet to be fully explored. In addition, we have studied other classes of

configurations for the purpose of finding ways to improve further the attractiveness of the quasi-axially symmetric stellarators. We have developed configurations of two field-periods with very small aspect ratios, making reactors of higher power densities and smaller sizes than the baseline possible. We made the shape simpler for these configurations in order to reduce the complexity of coils. We have also developed configurations with carefully chosen rotational transform profiles to minimize the effects of rational surfaces at high plasma pressures. These advanced configurations require additional investigation, but we believe that they have the potential to further improve the attractiveness and competitiveness of stellarator power plants. Moreover, we believe that an equally important outcome in our studies is the discovery of the richness of QAS configurations that offers us many different possibilities in designing future devices.

In spite of the progress we have made there are still needs for reducing the α loss further and making the flux surfaces more robust in our configurations. Coils should be further optimized and improved to reduce the complexity. We have found on many occasions that the optimized design is a compromise due to various imposed constraints. Many of these constraints are based on the incomplete knowledge such as the applicability and adequacy of the linear, ideal MHD in the determination of the beta limit. This led us to formulate a set of R&D needs to help resolve some of the design issues and uncertainties. With the new QAS device NCSX under construction, we hope that experiments in coming years will be able to establish a physics database that will help us clarify many of the design issues and will enable us to design even better compact stellarator reactors.

ACKNOWLEDGMENT

This work was supported by the United States Department of Energy Contracts DE-AC02-76-CHO-3073 (PPPL), DE-FG02-86ER53223 (CIMS), DE-AC05-00OR22725 (ORNL), DE-AC03-98ER54411 (GA) and DE-FC03-95-ER54299 (UCSD). We would like to thank Dr. A. Cooper, Dr. S. P. Hirshman, Dr. R. Sanchez, Dr. A. Reiman, and Dr. R. White for providing the computer codes TERPSICHORE, VMEC, COBRA, PIES and ORBIT3D, respectively.

.

REFERENCES

[1] A. WELLER, J. GEIGER, M. ZARNSTORFF, et al., *IAEA Nuclear Fusion and Plasma Phys.*, EX/S3-1, Lyon, France (2002).

[2] A. KOMORI, T. MORISAKI, T. MUTOH, et al., *Fusion Sci. Technol*., 50(2), 136 (2006).

[3] A. BOOZER, *Phys. Fluids*, 24(11) 1999 (1981).

[4] J. NUHRENBERG and R. ZILLE, *Phys. Lett*, 129A(2) 113 (1988).

[5] P. G. MATHEWS et al., *Proc. 10th Int. Conf. On Stellartors*, Madrid (1995).

[6] J. NUHRENBERG, W. LOTZ and S. GORI, *Theory of Fusion Plasma*, Varenna (1994), Editrice Compositori, Bologna 3 (1994).

[7] P. R. GARABEDIAN, *Phys. Plasmas*, 3, 2483 (1996).

[8] J. LYON, J. ROME, P. GARABEDIAN, and D. ANDERSON, *Proc. 15th International Conference on Plasma Physics and Controlled Nuclear Fusion Research*, Seville, 1994 (International Atomic Energy Agency, Vienna, 1996).

[9] R. L. MILLER, F. NAJMABADI, et al., UC San Diego Report UCSD-ENG-004 (1997).

[10] G. H. NEILSON, M. ZARNSTORFF, L. P. KU, et al., *19th International Atomic Energy Agency Fusion Energy Conference*, Lyon, France, October 14-19 (2002).

[11] A. S. WARE, S. P. HIRSHMAN, D. A. SPONG et al., *Phys. Rev. Lett.* 89, 125003 (2002).

[12] C. BEIDLER, G. GRIEGER, F. HERRNEGGER, et al., *Fusion Technol.,* 17, 148 (1990).

[13] A. SAGARA and O. MOTOJIMA, *Fusion Technol.*, 34, 1167 (1998).

[14] C. D. BEIDLER, E. HARMEYER, F. HERRNEGGER, et al., *Nucl. Fusion*, 41(12), 1759 (2001).

[15] L. P. KU and P. R. GARABEDIAN, *Fusion Sci. Technol*., 50, 207 (2006).

[16] S. SUDO, Y. TAKEIRI, H. ZUSHI, et al., *Nucl. Fusion*, 30, 11 (1990).

[17] J. MIYAZAWA, et al., *Nucl. Fusion*, 46, 532 (2006).

[18] J. LYON, L. P. KU, L. EL-GUEBALY, L. BROMBERG, et al., *Fusion Sci. Technol*., This issue.

[19] H. MYNICK, L. P. KU and A. BOOZER, *Phys. Plasmas*, 13, 064505 (2006).

[20] L. EL-GUEBALY, P. WILSON, et al., *Fusion Sci. Technol*., This issue.

[21] NCSX Engineering Design Review, "Design Description Conventional Coils and Structure," http://ncsx.pppl.gov/NCSX_Engineering/Technical_Data (2006).

[22] F. BAUER, O. BETACCOURT and P. GARABEDIAN, *Magnetohydrodynamic Equilibrium and Stability of Stellarators*, Springer-Verlag, New York (1984).

[23] G. Y. FU, L. P. KU, W. A. COOPER, et al., *Phys. Plasmas*, 7(5), 1809 (2000).

[24] P. R. GARABEDIAN and L. P. KU, *Phys. Plasmas*, 6, 645 (1999).

[25] D. STRICKLER et al., *IAEA Nuclear Fusion and Plasma Phys.*, FT/P2-06, Lyon, France (2002).

[26] S. P. HIRSHMAN, W. I. VAN RIJ and P. MERKEL, *Comp. Phys. Commun*, 43, 143 (1986).

[27] M. TAYLOR, *J. Comp. Phys*., 110, 407 (1994).

[28] A. H. REIMAN and H. GREENSIDE, *Comp. Phys. Commun*. 43, 157 (1986).

[29] V. V. NEMOV, S. V. KASILOV, W. KERNBICHLER and M. F. HEYN, *Phys. Plasmas*, 6(12), 4622 (1999).

[30] R. B. WHITE and M. S. CHANCE, *Phys. Fluids,* 27, 2455 (1984).

[31] D. V. ANDERSON, W. A. COOPER, R. GRUBER, S. MERAZZI, U. SCHWENN, *Scient. Comp. Supercomp. II*, 159 (1990).

[32] R. SANCHEZ, S. P. HIRSHMAN, J. C. WHITSON, and A. S. WARE, *J. Comp. Phys*. 161, 589 (2000).

[33] P. GARABEDIAN and M. TAYLOR, *Nucl. Fusion*, 32, 265 (1992).

[34] S. GORI, J. NUHRENBERG, R. ZILLE, et al., *Plasma Phys. Contr. Fusion*. 43, 137 (2001).

[35] A. A. SUBBOTIN, M. I. MIKHAILOV, J. NUHRENBERG, et al., *28th EPS Conference on Contr. Fusion and Plasma Phys.* Madeira, Portual, June 18-22 (2001).

[36] U. STROTH, et al., *Nucl. Fusion*, 39, 11 (1996).

[37] P. MERKEL, *Nucl. Fusion*, 27(5), 867 (1987).

[38] D. J. STRICKLER, L. A. BERRY and S. P. HIRSHMAN, *Fusion Sci. Technol*., 41, 107 (2002).

[39] S. C. JARDIN, C. E. KESSEL, C. G. BATHKE, et al., *Fusion Eng. & Des.*, 38, 27 (1997).

[40] K. WATANABE, N. NAKAJIMA, M. OKAMOTO, et al., *Nucl. Fusion*, 32(9), 1499 (1992).

[41] A. REIMAN, L. P. KU, D. MONTICELLO, et al., *17th IAEA Fusion Energy Conference*, IAEA-CN-69, Yokohama, Japan, 19-24 October (1998).

[42] M. ZARNSTORFF, A. WELLER, J. GEIGER, et al., *20th International Atomic Energy Agency Fusion Energy Conference*, EX/3-4, Vilamoura, Portugal, November 1-6 (2004).

[43] G. Y. FU, *Phys. Plasmas*, 7(4), 1079 (2000).

[44] G. Y. FU, L. P. KU, M. H. REDI, et al., *18th IAEA Fusion energy Conference*, Sorrento, Italy, 4-10 October (2000).

[45] P. GARABEDIAN, L. P. KU, et al., *Fusion Sci. Technol*., 47, 400 (2005).

[46] H. YAMADA, J. H. HARRIS, A. DINKLAGE, et al., *Nucl. Fusion*, 45, 1684 (2005).

[47] E. STRUMBERGER, *Nucl. Fusion*, 37, 19 (1997).

[48] K. BORRASS, *Nucl. Fusion*, 31, 1035 (1991).

[49] R. MANGI, Private Communication.

[50] T. K. MAU, T. KAISER, A.A. GROSSMAN, et al. *Fusion Sci. & Technol*., this issue.

[51] M. ZARNSTORFF, et al., *33rd EPS Conference on Plasma Physics*, Rome, Italy, 19-23 June (2006).

Figure Captions:

Fig. 1. Top and perspective view of the last closed magnetic surface for the baseline plasma.

Fig. 2. Four cross sections spaced at equal intervals over half a period of the baseline plasma.

Fig. 3. Contours of |B| of the baseline plasma on the flux surface at r/a~0.7 plotted in the normalized toroidal (horizontal) and poloidal (vertical) space showing the quasi-axisymmetric field structure, particularly in the outboard section. The contour values are scaled such that $B_{0,0}$ at the magnetic axis is 1.0 T

Fig. 4. Eight largest non-axisymmetric components in the magnetic spectrum of the baseline configuration as function of the normalized toroidal flux.

Fig. 5. |B| along a field line on the flux surface at r/a~0.7 of the baseline configuration for five poloidal transits starting from ϕ=0, θ=0 in the Boozer magnetic coordinate. The field strength is scaled such that $B_{0,0}$=1.0 T

Fig. 6. Top and side view of the baseline modular coils.

Fig. 7. Contours of distance from LCMS to the coil winding surface in the normalized poloidal/toroidal space for the baseline plasma and coils.

Fig. 8. Core components of ARIES-CS showing the winding support tube for modular coils and locations of PF coils.

Fig. 9. An example showing that the maximum magnetic field intensity in the coil body has a minimum with respect to the coil aspect ratio if the space needed for blanket/shielding is imposed as a constraint. The data shown here are based on a design of modular coils with topology similar to that given in Fig. 6 but with R~8.3 m and B_0~5 T. We have assumed that a thickness of 1.1 m is required for blanket/shield, plasma scrape-off, thermal insulation, coil case, etc. and that the remaining space available is used for the radial dimension of the coil conductor. The top curve is for conductors with square cross sections; the bottom curve is for conductors with a fixed width of 0.4 m.

Fig. 10. Flux surfaces of the baseline configuration at 5% β from a VMEC solution.

Fig. 11. Pressure (solid) and current density (dotted) profiles used for the equilibrium and MHD stability calculations.

Fig.12. Rotational transform profiles for the baseline configuration versus the normalized toroidal flux, s. Dotted line is the transform due to the deformation of the plasma surface. Solid line is the total transform including the contribution from the plasma current.

Fig. 13. Poincaré plot for the PIES solution of an equilibrium of the baseline plasma at 5% β.

Fig. 14. Comparison of a broad (dotted) current profile used in the kink stability studies with the baseline (solid) profile.

Fig. 15. Comparison of LCMS showing the additional boundary deformation needed to make the baseline configuration (solid) kink stable in the ideal, linear MHD limit at 5% β (dotted) when the broad current profile in Fig. 14 is used.

Fig. 16. Effective helical ripple as function of normalized toroidal flux for the baseline plasma.

Fig. 17. Energy loss fraction of alpha particles versus the collisionality parameter $\langle n \rangle R/\langle T \rangle^2$ for R=10 m (bottom curve) and R=7 m (upper curve). B_0=6.5 T. Here, $\langle n \rangle$ and $\langle T \rangle$ are the volume-averaged density and temperature.

Fig. 18. Footprint of the alpha particles leaving LCMS of the baseline configuration in (θ, ϕ).

Fig. 19. Frequency distribution of the energy of alpha particles left LCMS of the baseline configuration.

Fig. 20. Poincaré plots for MFBE solutions of the baseline configuration showing the topology of the magnetic field outside LCMS. In this calculation R=8.25 m was used.

Fig. 21. Four cross sections spaced at equal intervals over half a period of the A=2.5 MHH2 and top view of the associated modular coils designed with a coil aspect ratio 5.5.

Fig. 22. Eight non-axisymmetric components in the MHH2 magnetic spectrum with the largest magnitude as function of the normalized toroidal flux.

Fig. 23. Four cross sections spaced at equal intervals over half a period of the A=4.5 configuration with the specially tailored rotational transforms.

Fig. 24. Rotational transform profiles for the configuration shown in Fig. 23.

Fig. 25. Poincaré plot for the PIES solution of an equilibrium at 5% β for the configuration shown in Fig. 23.

Fig. 26. Four cross sections spaced at equal intervals over half a period for the A=6 configuration with a strong negative shear in the external transform.

Fig. 27. Rotational transform profiles for the configuration shown in Fig. 26.

Fig. 28. Poincaré plot for the PIES solution of an equilibrium at 6% β for the configuration shown in Fig. 26.

Fig. 29. Top and perspective view of a preliminary design of modular coils for the configuration shown in Fig. 26.

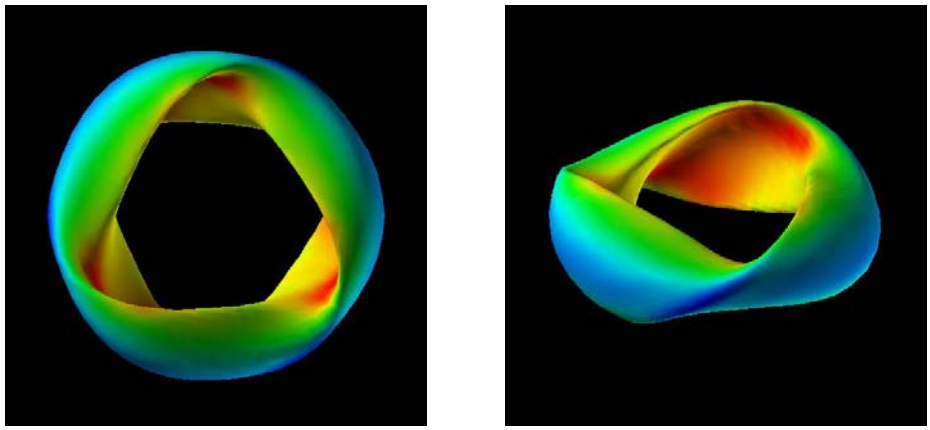

Fig. 1
L. P. Ku, et al, “Physics Design for ARIES-CS”

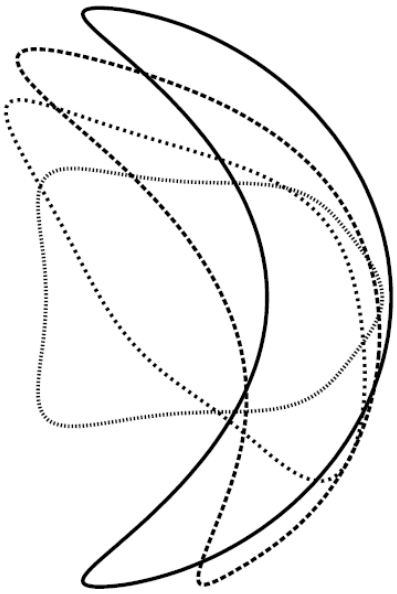

Fig. 2
L. P. Ku, et al, “Physics Design for ARIES-CS”

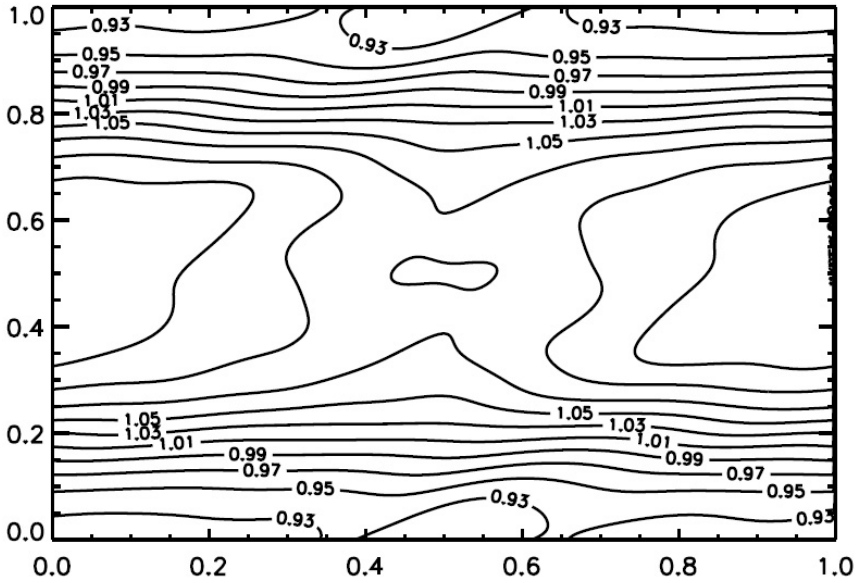

Fig. 3
L. P. Ku, et al, "Physics Design for ARIES-CS"

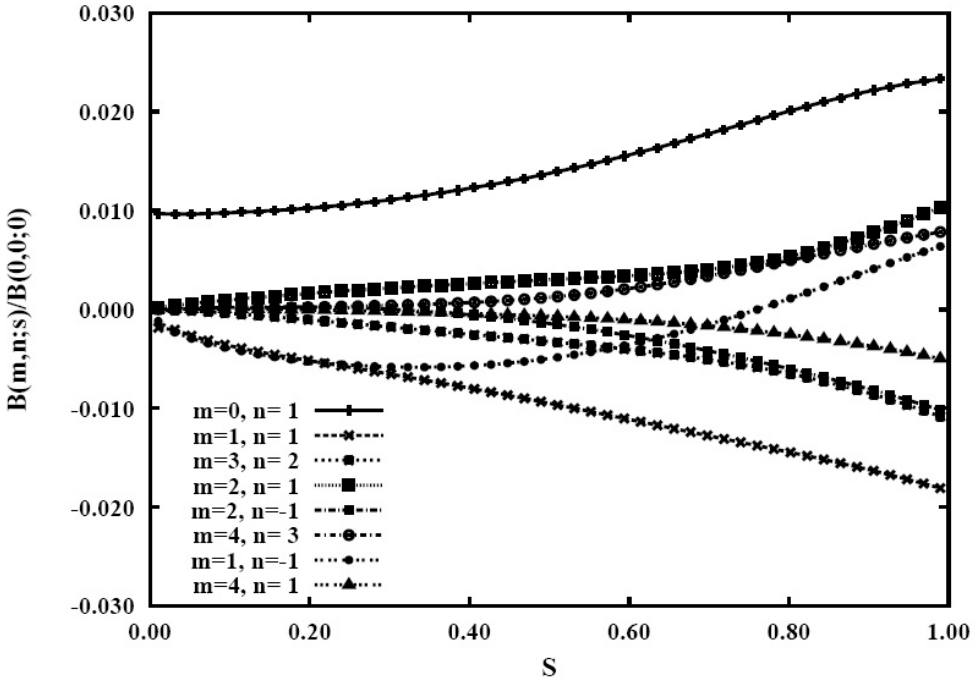

Fig. 4
L. P. Ku, et al, "Physics Design for ARIES-CS"

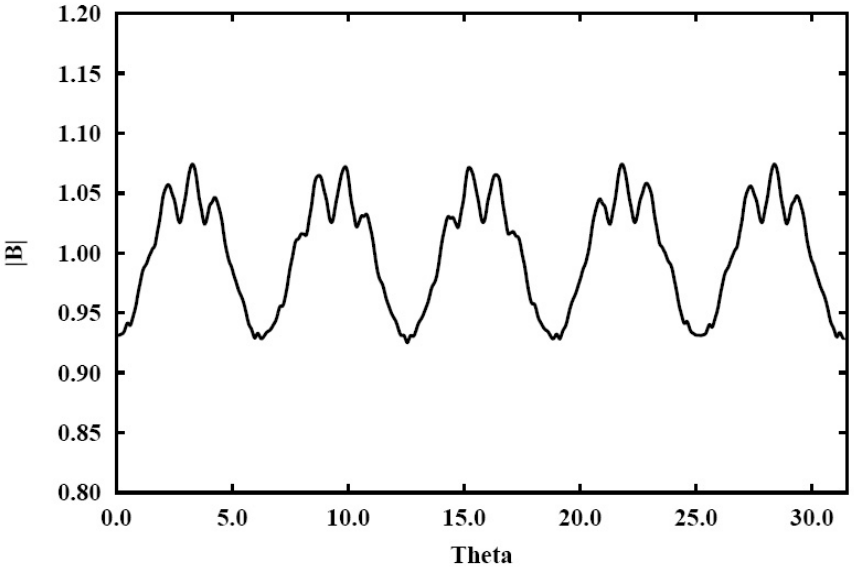

Fig. 5
L. P. Ku, et al, "Physics Design for ARIES-CS"

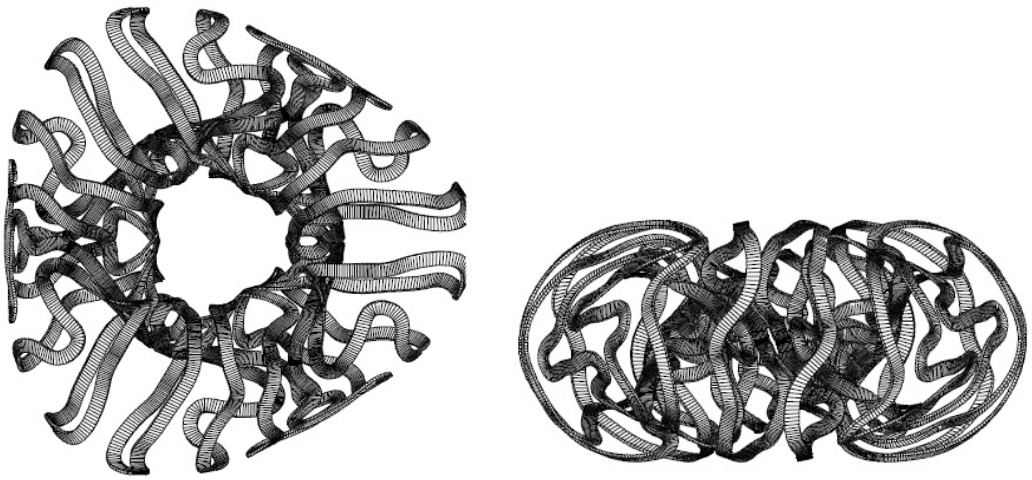

Fig. 6
L. P. Ku, et al, "Physics Design for ARIES-CS"

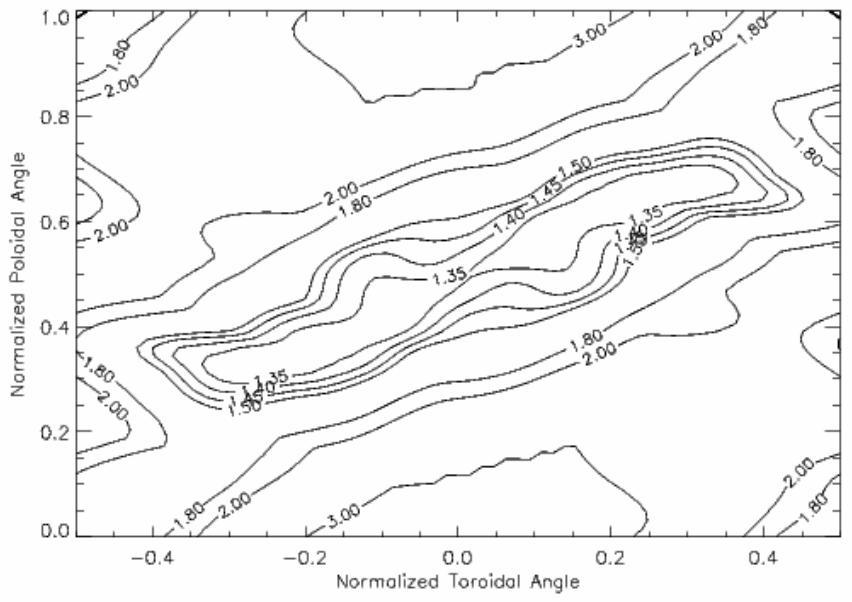

Fig. 7
L. P. Ku, et al, "Physics Design for ARIES-CS"

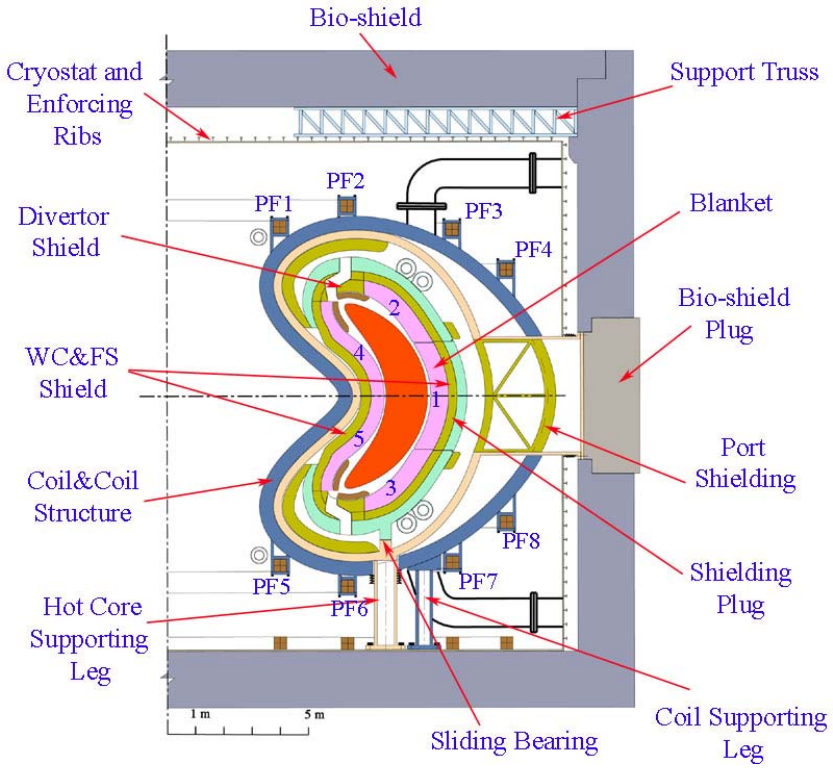

Fig. 8
L. P. Ku, et al, "Physics Design for ARIES-CS"

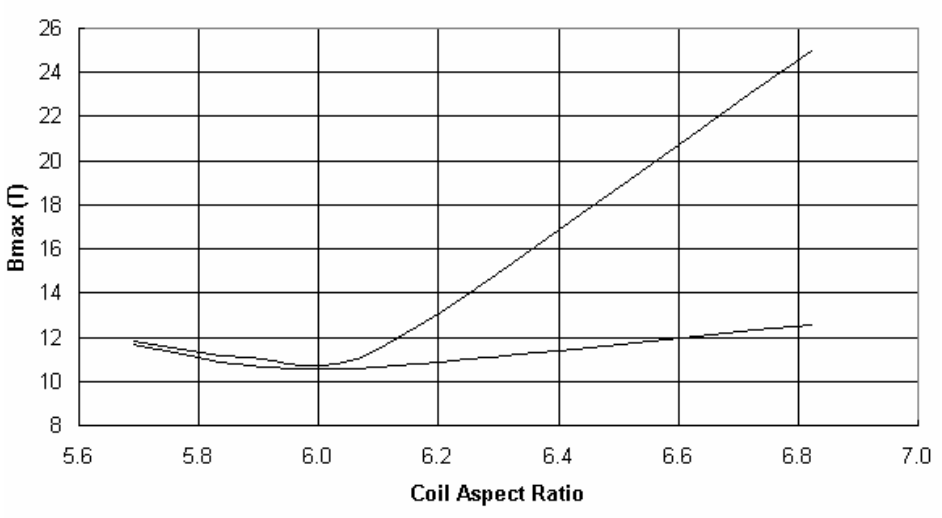

Fig. 9
L. P. Ku, et al, "Physics Design for ARIES-CS"

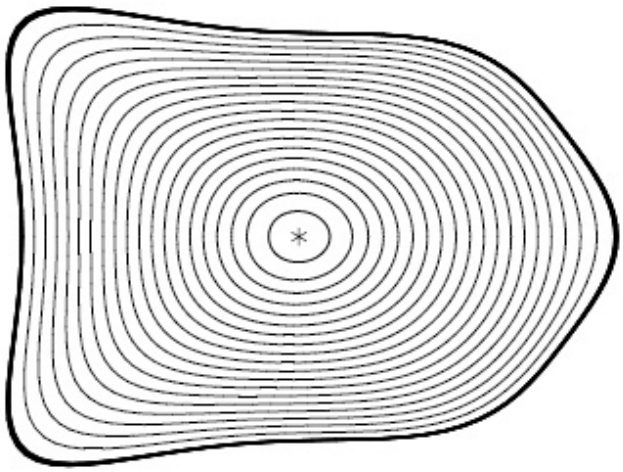

Fig. 10
L. P. Ku, et al, "Physics Design for ARIES-CS"

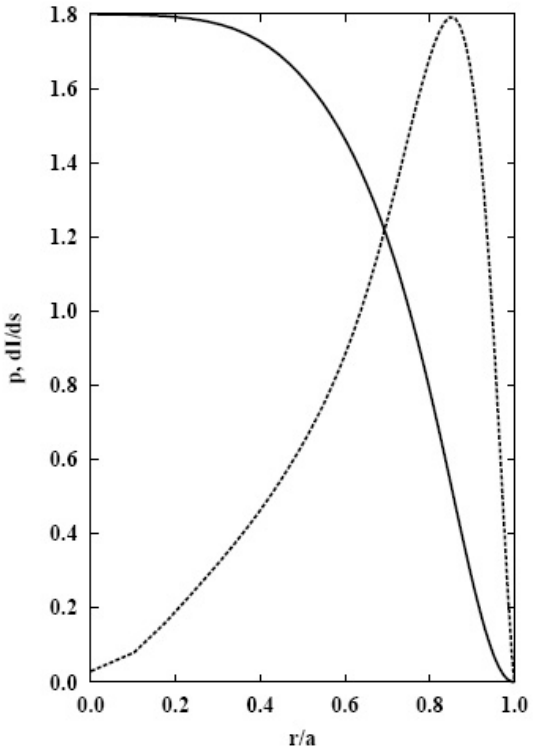

Fig. 11
L. P. Ku, et al, "Physics Design for ARIES-CS"

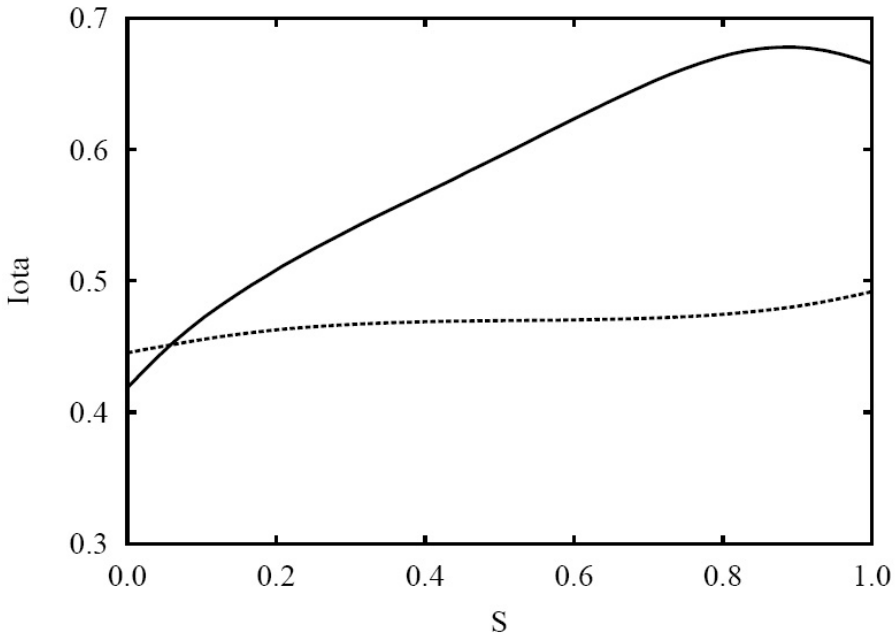

Fig. 12
L. P. Ku, et al, "Physics Design for ARIES-CS"

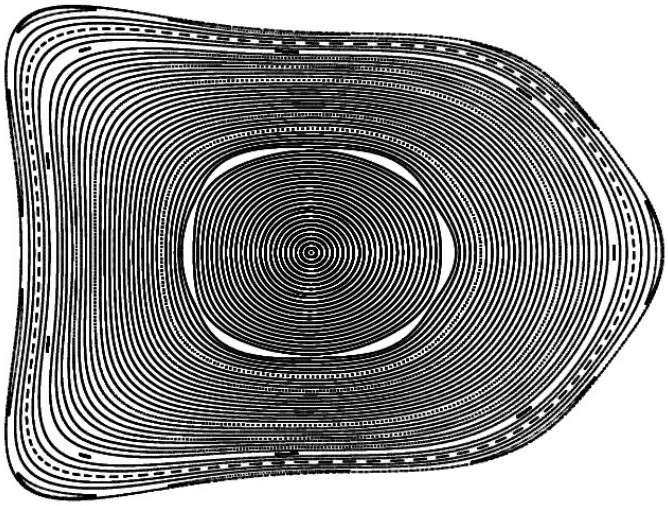

Fig. 13
L. P. Ku, et al, “Physics Design for ARIES-CS”

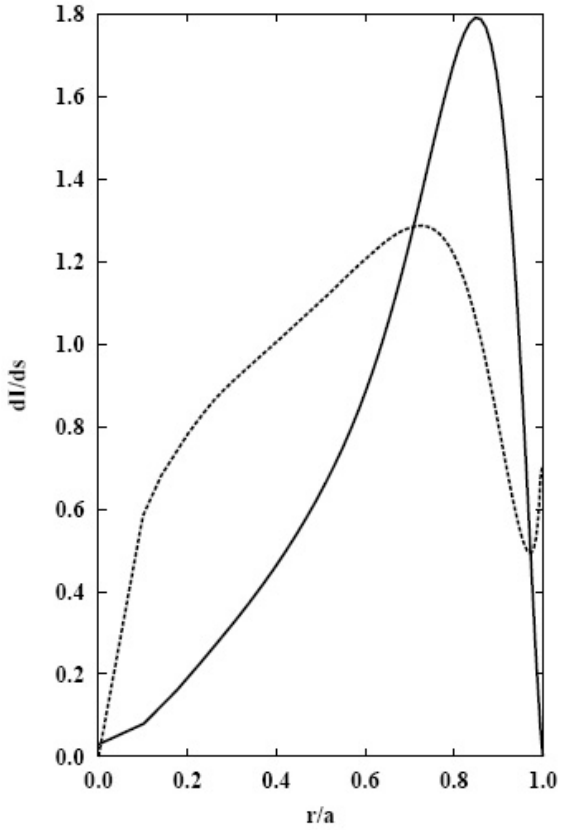

Fig. 14
L. P. Ku, et al, “Physics Design for ARIES-CS”

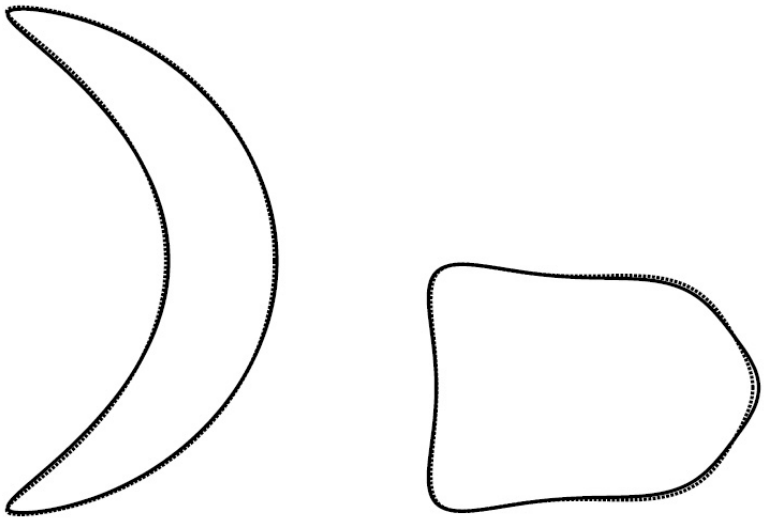

Fig. 15
L. P. Ku, et al, “Physics Design for ARIES-CS”

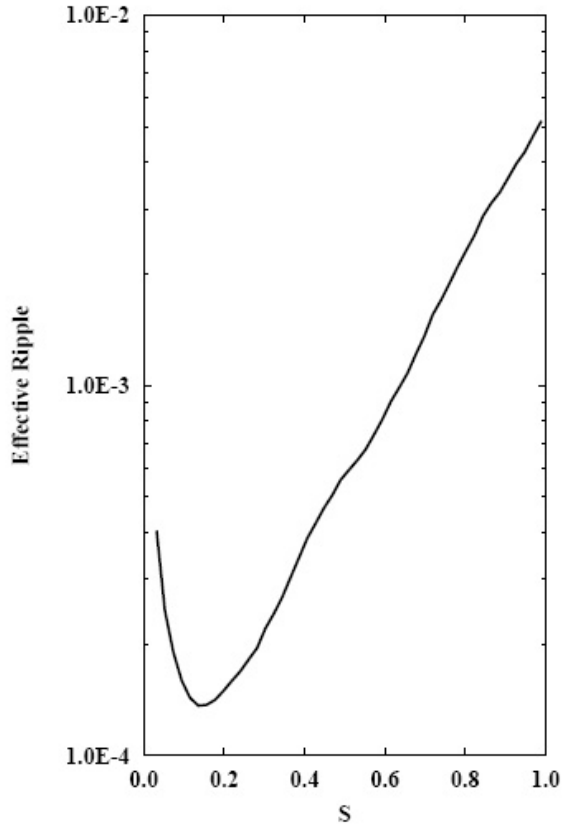

Fig. 16
L. P. Ku, et al, “Physics Design for ARIES-CS”

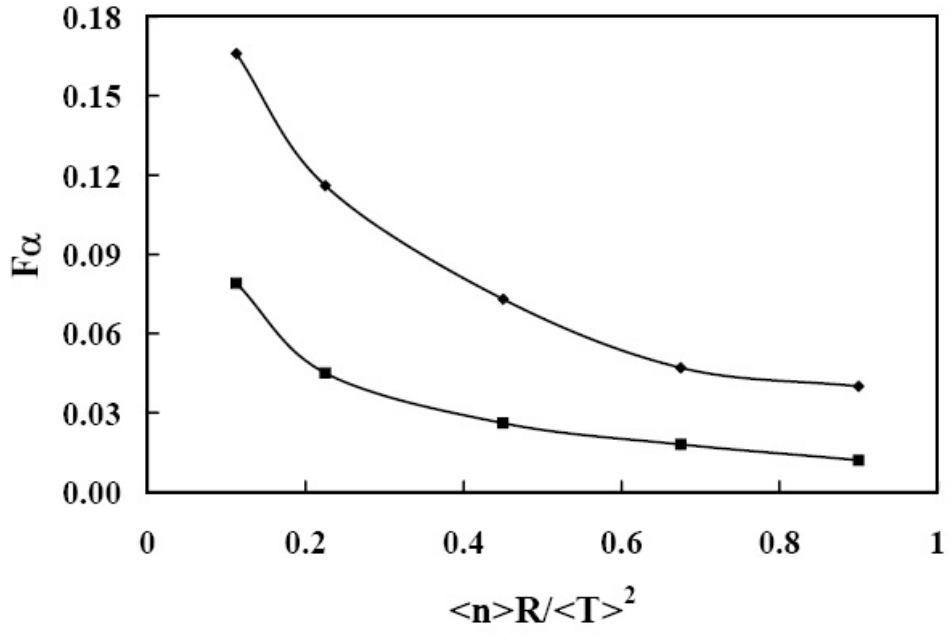

Fig. 17
L. P. Ku, et al, "Physics Design for ARIES-CS"

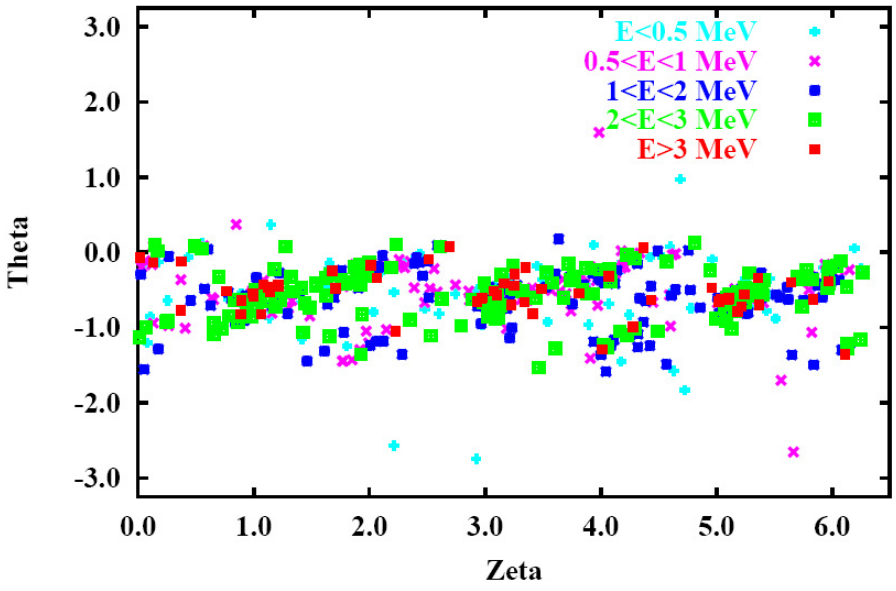

Fig. 18
L. P. Ku, et al, "Physics Design for ARIES-CS"

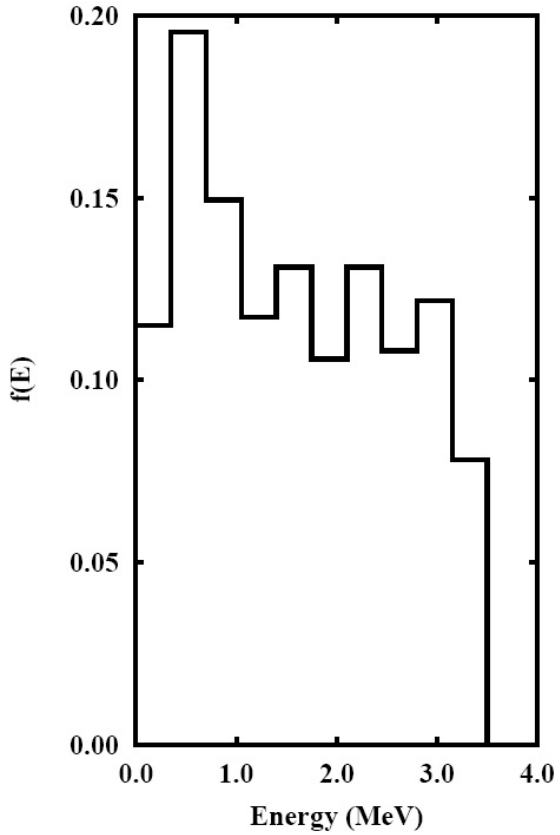

Fig. 19
L. P. Ku, et al, "Physics Design for ARIES-CS"

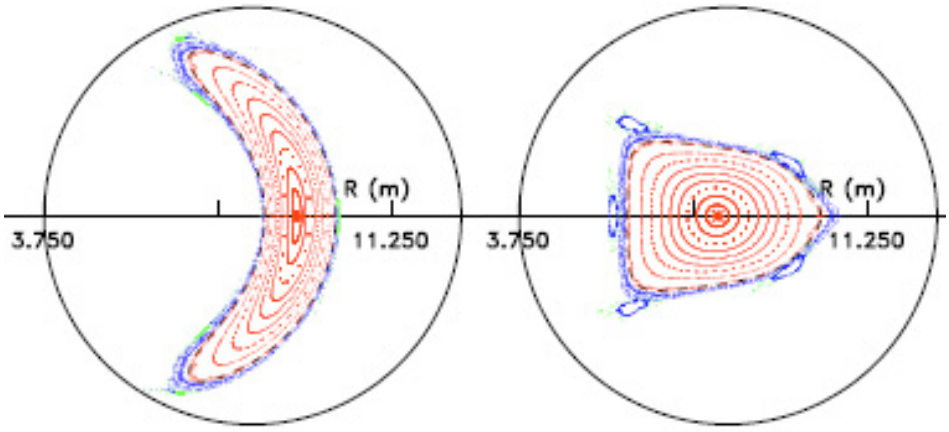

Fig. 20
L. P. Ku, et al, "Physics Design for ARIES-CS"

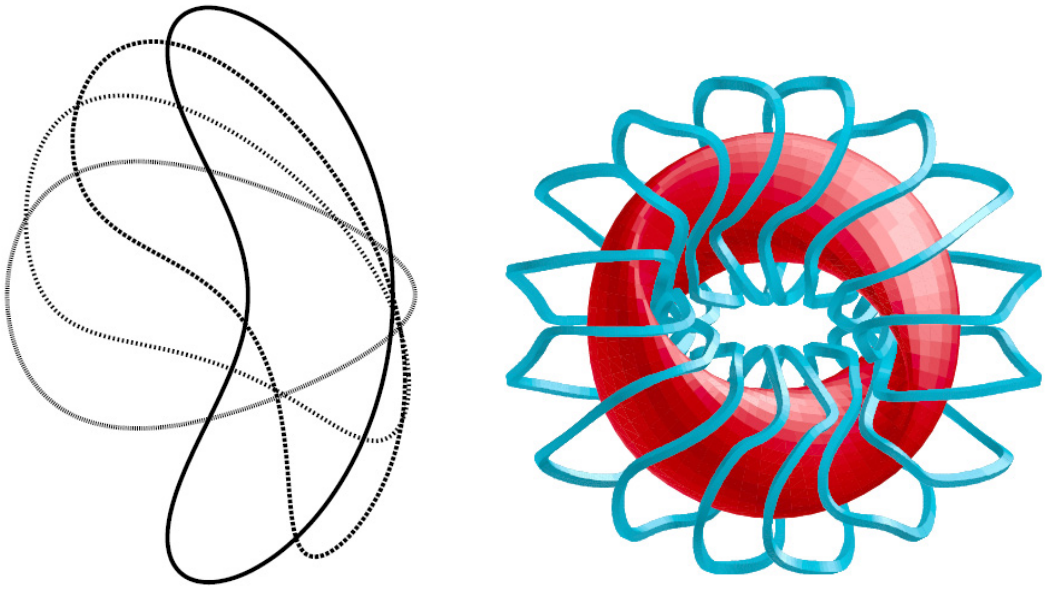

Fig. 21
L. P. Ku, et al, "Physics Design for ARIES-CS"

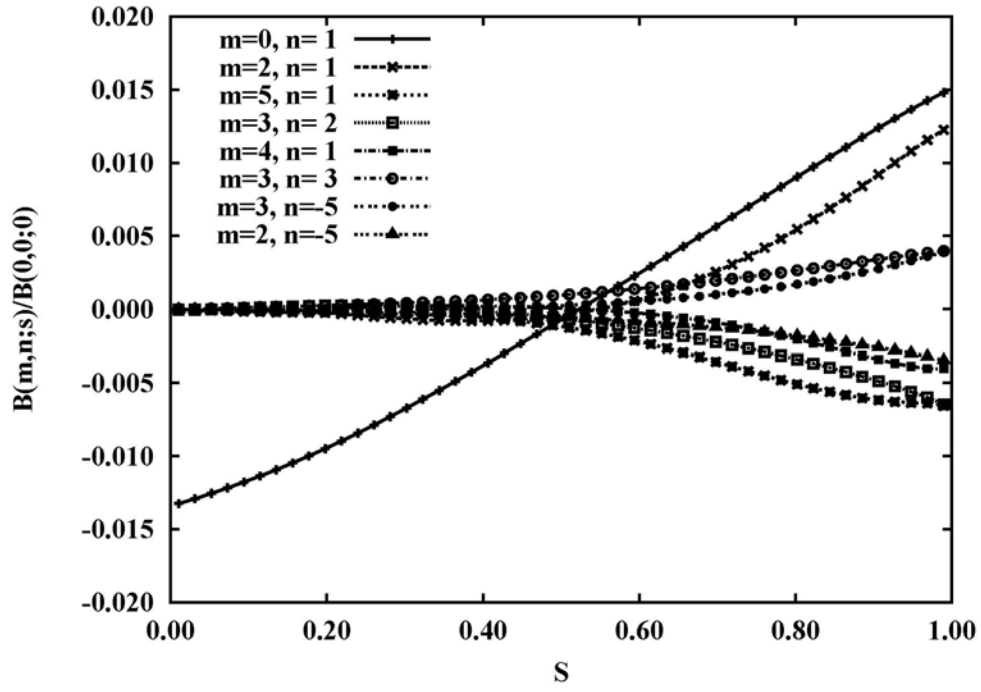

Fig. 22
L. P. Ku, et al, "Physics Design for ARIES-CS"

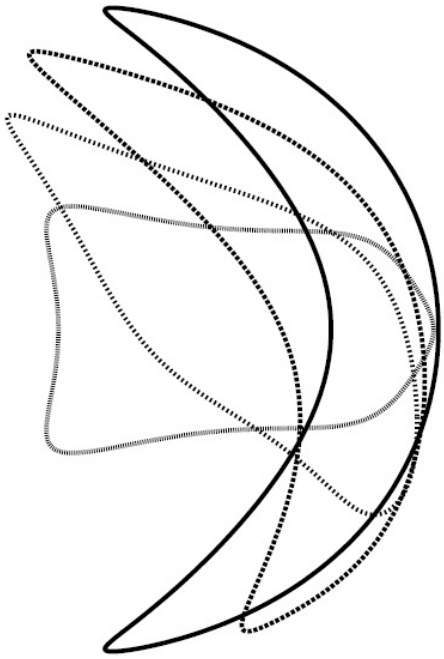

Fig. 23
L. P. Ku, et al, “Physics Design for ARIES-CS”

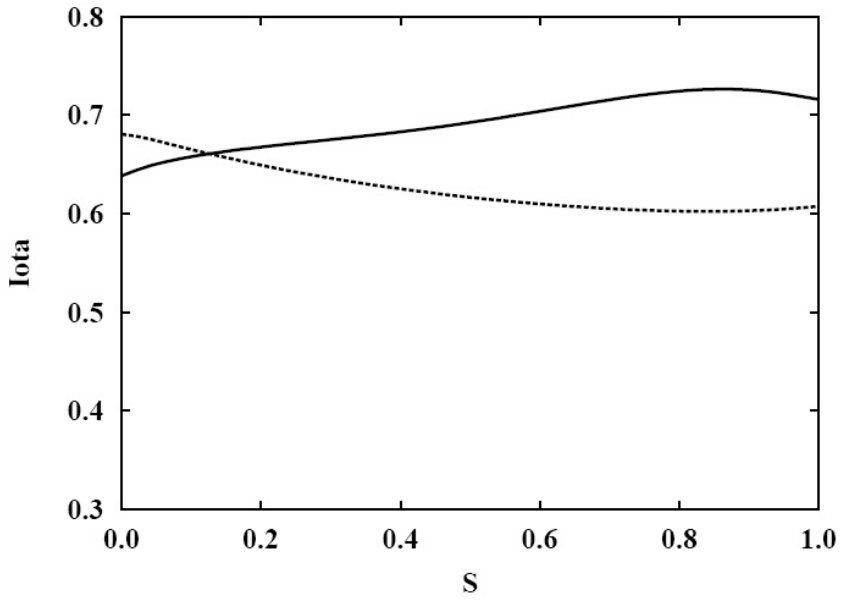

Fig. 24
L. P. Ku, et al, “Physics Design for ARIES-CS”

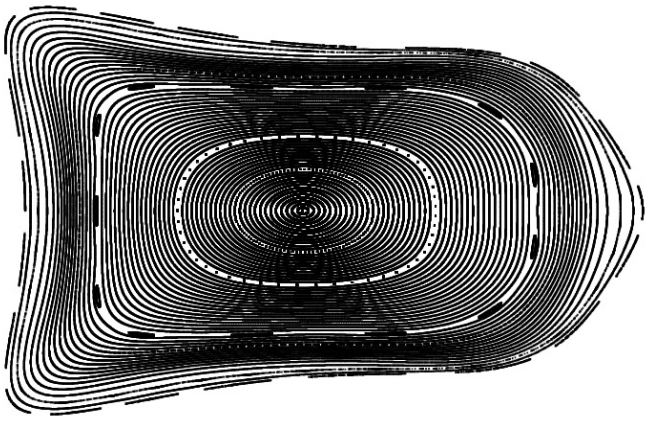

Fig. 25
L. P. Ku, et al, “Physics Design for ARIES-CS”

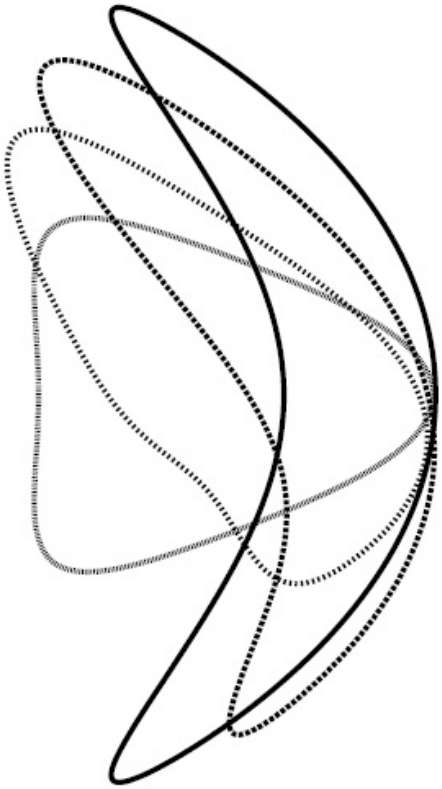

Fig. 26
L. P. Ku, et al, “Physics Design for ARIES-CS”

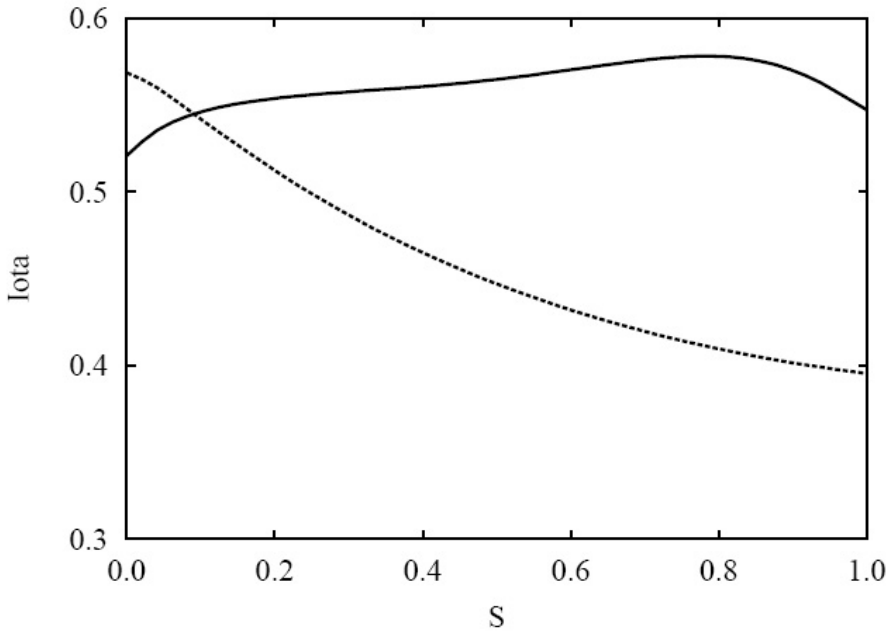

Fig. 27
L. P. Ku, et al, "Physics Design for ARIES-CS"

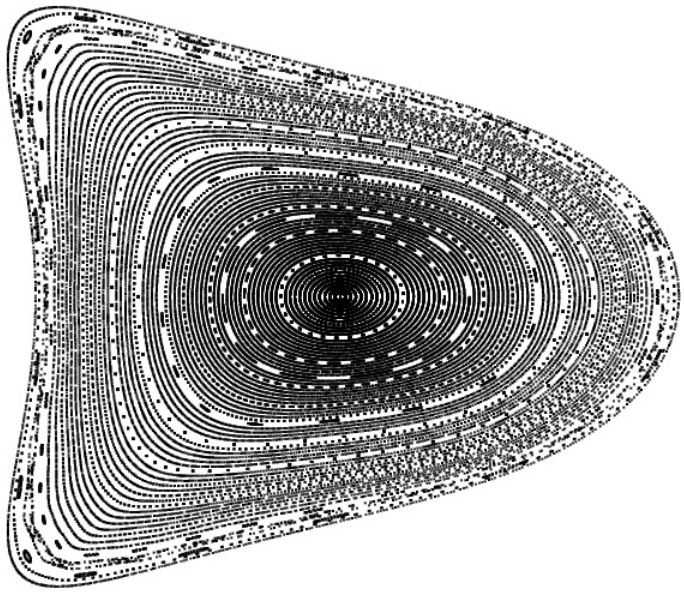

Fig. 28
L. P. Ku, et al, "Physics Design for ARIES-CS"

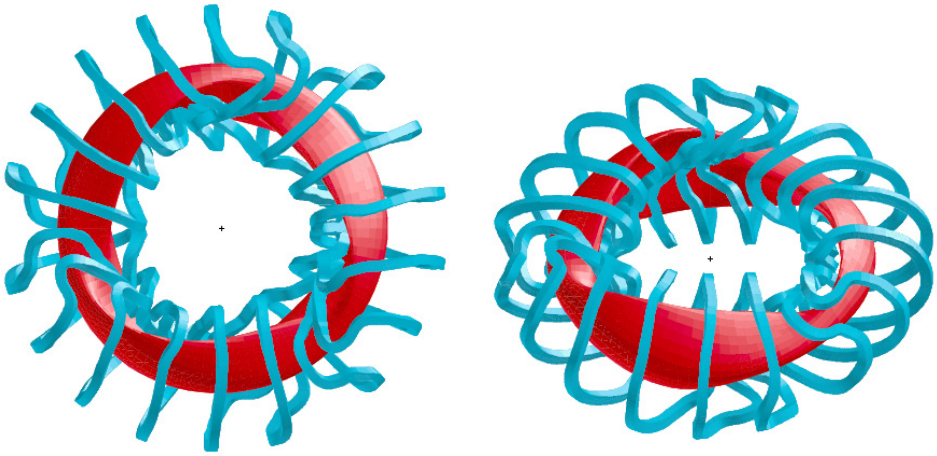

Fig. 29
L. P. Ku, et al, “Physics Design for ARIES-CS”

The Princeton Plasma Physics Laboratory is operated
by Princeton University under contract
with the U.S. Department of Energy.

Information Services
Princeton Plasma Physics Laboratory
P.O. Box 451
Princeton, NJ 08543

Phone: 609-243-2750
Fax: 609-243-2751
e-mail: pppl_info@pppl.gov
Internet Address: http://www.pppl.gov